INVESTIGATIONS ON METAL NANOPARTICLES INDUCED SURFACE MODIFICATIONS OF THIN FILM ELECTRODES FOR POSSIBLE APPLICATION IN PHOTOELECTROCHEMICAL WATER SPLITTING

Synopsis

Submitted in the partial fulfilment for the requirement of

Doctor Of Philosophy
In
Chemistry

Submitted by

Bhanupriya

Under the supervision of

Prof. Rohit Shrivastav
(Supervisor)
Head, Department of Chemistry

Department of Chemistry, Faculty of Science
Dayalbagh Educational Institute (Deemed to be a university)
Dayalbagh, Agra-282005

2022

1. Introduction

The economic stability and growth of any nation depend directly or indirectly on the availability and supply of energy. These energy systems in a society are interwoven and include the production of energy in various forms for the effective use of resources, the consumption of energy by various sectors to meet the energy demands of vast populations, and its impact on the environment at any level. If there is a glitch at any of these levels, then there is a direct impact on the country's economy and development. Rising populations and urbanization have raised energy consumption almost exponentially in recent years. These demands are mostly met by energy generation through non-renewable resources such as fossil fuels, coal, oil, petrol, diesel, etc. The continued use of non-renewable and limited resources has put the world in the scarcity of such resources and our future generations may be deprived of these. At the same time, the environment is also severely affected by their continued use as various pollutants are emitted on their consumption. Hence, the world is looking for a clean and renewable replacement of conventional energy reserves and a comprehensive investigation is underway to enable large-scale usage of renewable sources of energy. Researchers are focusing on the long-term, sustainable, clean, carbon-free fuels in reasonable expense that would transform fossil fuel dominateed economy to a green economy. The International Energy Agency report (2019) states that world energy demand will double by the year 2040 and renewable sources are expected to supply only 7% of total world energy demand. IEA World Energy Outlook Report (2020), which considers the impact of the COVID-19 pandemic on world energy demand, says that this situation would change the future of energy for years to come. They say that it is timely to mention whether this crisis is a barrier to safe and sustainable energy system efforts, or a catalyst that accelerates the path of change. But they are hoping that the demand for coal will not return to pre-epidemic levels, and it will account for less than 20% of energy consumption by 2040, this could prove to be a great time for renewables to handle the entire landscape. They further predict that in the coming decades, renewables will take "starring roles", and solar will take "center stage". In view of this, hydrogen is turning into the most futuristic fuel that can store and distribute energy derived from renewable sources, especially solar energy. Hydrogen has many valuable properties; viz. higher

energy per unit mass compared to other fuels such as methanol, diesel, and gasoline; higher heat of combustion than petroleum; higher energy storage capacity/mol than oil; and combustion of hydrogen fuel being environmentally banign, producing the harmless substance water. Keeping all these properties in mind, hydrogen has the potential to replace fossil fuels. Solar-hydrogen production by water splitting is a convenient and green way to provide efficient fuel. This solar water splitting to produce hydrogen can be carried out in different ways such as photovoltaic electrolysis (PV), photo-catalysis, and photoelectrochemical (PEC) water splitting. PEC along with its intrinsic valuable mileage over the other technique is developing as the pivotal method for the generation of hydrogen from the ubiquitous renewable resources i.e. water and sunlight.

2. Photoelectrochemical water splitting: Background and significance

Photoelectrochemical water splitting (PEC), which involves the combinatorial action of solar power and water splitting, has provided an efficient way to produce renewable hydrogen. First demonstration of the PEC water splitting was initiated within the mid-70s on the TiO_2 semiconductor (Fujishima et al., 1972). Thenceforward, the appetency to separate water for hydrogen generation has struggled with its challenges that are rooted in its material design, cell design, efficiency improvement, and commercial viability. In the nutshell, PEC water splitting involves conversion of solar energy into electrical energy, which is further used to decompose water to produce hydrogen. The specific cell design required for this reaction may have two types of configurations. One of the configurations consists of photoanode or photocathode (made of semiconductor material), counter electrode (anode/cathode), and electrolyte. In another type of configuration, both anode and cathode are made of semiconductor material and this configuration can be called a tandem cell consisting of photoanode, photocathode, and electrolyte. The latter configuration is the emerging one, which can provide self-sufficient and stand-alone cell-design; while the former is the primary one, which explains the basic mechanism of the PEC cell.

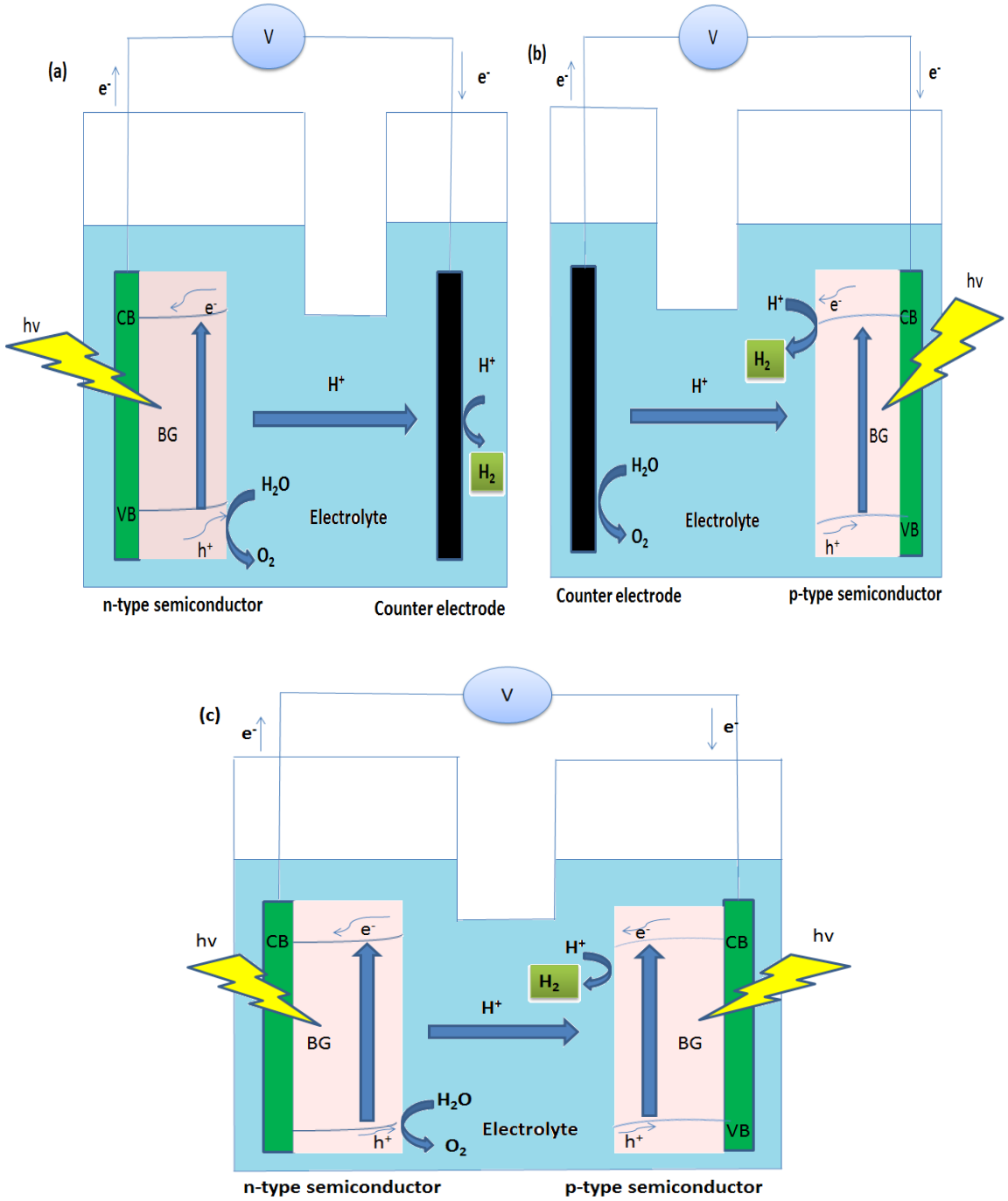

Fig. 1 Different configurations of Photoelectrochemical cell for water splitting: (a) Working electrode is n-type semiconductor which behaves as photo-anode, (b) Working electrode is p-type semiconductor which behaves photo-cathode, (c) Tandem cell configuration where both electrodes are photoelectrodes.

The basic mechanism of PEC cell containing photoanode involves the following steps: (i) absorption of sunlight by photoanode leading to the excitation of electrons from the valence band to the conduction band, which results in the production of exciton pairs, (i) absorption of sunlight by photoanode leading to the excitation of electrons from the valence band to the conduction band, which

results in the production of exciton pairs, (ii) the holes react with the water to generate hydronium ion and oxygen, (iii) the electron from the photoanode transferred to the cathode by external wires while the hydronium ion transfer to the cathode through the electrolytic solution, where the reduction of hydronium ion to form hydrogen take place by electrons.

Photoanode + Sunlight $(h\nu)$ $\rightarrow$ $2e^-$ + $2h^+$

At photoanode (oxidation): $H_2O\ (l)$ + $2h^+$ $\rightarrow$ $\frac{1}{2}\ O_2\ (g)$ + $2H^+$

At cathode (reduction): $2H^+$ + $2e^-$ $\rightarrow$ $H_2\ (g)$

The decomposition reaction of water is a non-spontaneous reaction that is thermodynamically non-accessible on its own. The decomposition of water requires an external potential of 1.23 eV (Fujishima et al., 1972), and this can only occur when the bandgap of a semiconductor material is equal to or greater than 1.23 eV. But practically for efficient and sustainable photoelectrolysis of water, the required bandgap is between ~ 1.8-2.4 eV, as inherent phenomenon such as energy losses and over-potential losses also persist. Collectively, there are several critical aspects that are involved in the mechanism of PEC water splitting, such as light absorption and charge segregation, charge recombination in bulk and at the surface, charge transfer and transport at interfaces, and surface redox reactions. On this basis, besides having an optimum bandgap, there are many other conditions that should be fulfilled by a semiconductor for behaving as an efficient photoelectrode. (i) The semiconductor should have proper band edge position w.r.t. water redox potentials i.e. the conduction band should be at more negative potential than water reduction potential to perform hydrogen evolution reaction and valence band should be at more positive than water oxidation potential to perform oxygen evolution reaction. (ii) The semiconductor should provide good interfacial charge transfer reaction to prevent charge recombination. (iii) Semiconductor should show high photochemical stability by being resistant towards photo-corrosion and electrolytic corrosion. (iv) Semiconductor must be low-cost and readily available material. In the past few decades, many semiconductors have been intensively studied such as TiO_2, ZnO, WO_3, Fe_2O_3, and $BiVO_4$. All these have their merits and demerits towards the PEC water splitting. A number of modifications and strategies have also been implemented to overcome these shortcomings.

3. Progress so far: A glimpse through literature

From the very first report on PEC water splitting by Fujishima and Honda, PEC water splitting has shown great potential for renewable hydrogen generation. A lot of research has already been done over different semiconductor, which may now be regarded as first generation semiconductors for PEC water splitting, such as TiO_2 (~3.2 eV) (chai et al., 2019), ZnO (~3.37 eV) (Kegel et al., 2018), WO_3 (2.5-2.8 eV) (Wang et al., 2019), Fe_2O_3 (~2.1 eV) (Tamirat et al., 2016) and Cu_2O (1.9 eV-2.17 eV) (Begal et al., 2019). These metal oxides have gained importance in PEC water splitting owing to their easy availability and high stability. But, using metal oxides have been inflicted with several drawbacks/dilemmas as well. For instance, wide bandgap metal oxides are mostly stable, but they can only absorb only restricted portion of solar spectrum i.e. UV light. On the other hand, small bandgap semiconductors can make ulitization of wider portion of solar spectrum including visible region but they suffer from poor stability in electrolytes. Semiconductors such as Fe_2O_3 which are free from these two limitations have another problem of rapid charge recombination rates and short carrier diffusion length. Over a period of intense research, besides metal oxides many other materials have also been investigated such as $CuBi_2O_4$, GaP, GaN, InGaN, InP, CdS, Ta_3N_5, InAs, $CuInS_2$, g-C_3N_4 etc. But till now, none of the explored material has provided the remarkable PEC efficiency for its market implementations. So, to extricate intrinsic problems of these materials, several modification strategies have been adopted by researchers such as dimensionality modifications(1D, 2D, 3D & 0D), metal or non-metal doping and co-doping, quantum dots sensitization (CdS, CdSe, PbS, CQDs, GQDs, Cu_2S, $AgInS_2$ QDs, Bi_2WO_6 QDs, MoS_2 QDs), co-catalyst incorporation (Co-Pi, Fe-Pi, $Ni(OH)_2$, ZnFe-LDH, NiFe-LDH, NiMn LDH, NiOOH), homo and hetero-junction formation, passivation technique, and nanostructure and hetero-nanostructure designing etc. In the recent few years, the formation of multi-integrated photoelectrode i.e. incorporation of several strategical approaches in designing the photoelectrode is flourishing splendidly. Cao and his colleagues (Cao et al., 2016) have designed nanostructured photoanode in which $ZnFeO_3$ (ZFO) nanoparticles were deposited over CdS QDs/ZnO NRs core/shell structure. This composite contained type II heterojunction between these three units, which improved the charge separation efficiency; while quantum dot sensitization along with deposition of ZFO increased the light absorption ability of photoanode. Moreover, ZFO acted as hole-

extractor and passivation support for photo-corrosive CdS quantum dots. The result of this combination was remarkable with photocurrent density of 3.88 mA/cm^2 at 0 V vs Ag/AgCl and STH efficiency of 4.4 %. In the same year, Liu (Liu et al., 2016) has shown a highly efficient and cost effective combination of nanosheet and nanorod arrays to make sandwiched photoelectrode, TiO_2/CdS/$ZnIn_2S_4$. At optimum conditions, this combination showed photocurrent density 9.33 mA/cm^2 at 0.53 V with proper band alignments. The one dimensional (1D) nanorods provided direct electrical pathways for photo-induced electrons. Indroduction of CdS buffer layer decreased the recombination rate of interface electrons by inhibiting recombination centers (traps and defect states). The nanosheets (2D) of $ZnIn_2S_4$ acted as the passivation layer to prevent photocorrosion of CdS. The co-sensitization of quantum dots over branched nanorod arrays (BNRs) provided a unique way to design a photoelectrode with efficient performance. TiO_2 BNRs/CdS/Cu_2S exhibited photocurrent density 13.65 mA/cm^2 at 0 V vs Ag/AgCl, along with hydrogen generation efficiency 7.74% at -0.467 V. The heterojunction formed between CdS and Cu_2S enhanced the flow and separation of photo-induced electrons (Tang et al., 2016). The ternary heterostructure of GaN/ZnO/MWCNTs photoanode was synthesized by Patil and his cowokers (Patil et al., 2018). GaN and ZnO are highly subsidiary to one another, as they have same wurtizite structure. The II type heterojnction formed between GaN and ZnO provided the way to reduce recombination and promote transportation and separation of electron hole pair. MWCNTs played a very crucial role in enhancing light harvesting ability in visible region as well as in improving surface morphology of the photoanode. This combination resulted in the photocurrent density of 3.02 mA/cm^2 at 0 V. Subramanyam and his co-workers (Subramanyam et al., 2018) have prepared Mo-doped and reduced graphene oxide (rGO) covered $BiVO_4$ photoanode. Mo doping increased the carrier charge density and rGO decoration accelerated the transfer and collection of excitons. The highest photocurrent density exhibited was 8.51 mA/cm^2 at 1.23 V_{RHE}. It was demonstrated that this composite showed increased PEC performance and higher photo-stability than doped and un-doped $BiVO_4$. Far from all these aforementioned complex strategies, Alvi et al (2019) developed an easily fabricated and cost-effective photoelectrode which they were claimed to provide economic viability. They prepared InGaN nanowalls over Si substrate decorated with InN quantum dots. They set a record for a single photoelectrode to provide unassisted PEC water splitting with

photocurrent density of 18.2 mA/cm^2, IPCE value of 74%, and light-to-hydrogen power conversion efficiency of 9.3% under white light illumination at zero external bias. This photoelectrode showed high stability for 10 h irradiation time, which confirmed the great chemical stability of InGaN. In another report, III-IV group compound semiconductor InAs having narrow and direct bandgap and good electron mobility was used over Si to improve its kinetics (Choi et al., 2019). This InAs is very unstable at extreme pH, hence, they used a passivation layer of ALD-grown TiO_2 to protect it. The Pt/TiO_2/InAs NWs/*p*-Si photocathode was showing an enhanced photocurrent density of 8.6 mA/cm^2 at zero bias and great stability over 20 h at neutral pH. While forming the hetero-junctions, a binder persists in the form of interfacial resistance between solids leading to create obstacle in charge transfer and badly influence the stability of the photo-electrode. To surmount this problem a highly ordered three-dimensional mesoporous ZnO/$Zn_xCd_{1-x}Se$ inverse opal photoelectrode with binder-free heterojunction was demonstrated to provide maximum photocurrent density of 24.76 mA/cm^2 at 1.23 V in presence of sacrificial agents (Na_2S and Na_2SO_3) under optimized conditions. This hetero-structure was benefitted by $Zn_xCd_{1-x}Se$, which acted as photo-sensitizer for ZnO, and also the type II band alignment facilitated enhanced interfacial charge transfer by reducing resistance. The photostability and maximum photoconversion efficiency were also superior (Zeng et al., 2019). Wang et al (2020) have presented a paper in which they have used HER catalyst, NiFe-LDH (layered double hydroxide). First, they have prepared Cu_2O and then passivated it with TiO_2 to prevent its corrosion and also form heterojunction. Then, rGO/ NiFe-LDH composite catalyst was incorporated over the surface. The resulted Cu_2O/TiO_2/rGO/NiFe-LDH photocathode exhibited photocurrent current density of 3.71 mA/cm^2 at 0 V_{RHE}. With all these aforementioned expurgations, there is one more interesting modification technique, which is drawing excellent attention nowadays by the scientist. This is the use of plasmonic effects of metals in improving the PEC performances. Researcher are doing great work in designing the Plasmon-dominated photoelectrode that may provide a way forward to ameliorate with the hurdles that are coming in between development of the practical PEC devices. Plamonic metals are providing new paragon in this field, as they can be used as alternative photosensitizer, which have potential to solve problems associated with the other photosensitizers such as occurrence of unwanted defects and repugnant stability with the use of photosensitizers. The plasmonic metals

exhibit Surface Plasmon resonance phenomenon and have electron trapping ability that may improve STH efficiencies of PEC devices. They are gaining interest because of some unique characteristics like high absorption cross sections, expectional chemical stability, tunable size and geometry-dependent optical properties, visible and near infra-red light absorption, no adverse effect on electrical properties of the semiconductor (Lee et al., 2017).

4. Heterostructure architecturing

In recent years, heterostructures formation approach is providing better results as compared to single material photoelectrode, and also gaining more intensive research attention. This heterostructure formation approach can have two basic grounds for its implementation i.e. on the basis of morphology of the materials and on the basis of energy band alignments of different materials. Based on morphology, these heterostructures can be designed by having partial contact and full contact between two materials. The former design consists of point contact heterostrucures in which one material is in the form of nanoparticle (0D-0D, 0D-1D, 0D-2D), line contact heterostructures for nanowire and nanosheets (1D-2D), and face contact heterostructures having both as two dimensional materials (2D-2D). The latter design includes nanowire core- shell and sphere core-shell heterostructures (Low et al., 2017). In addition, depending upon the energy band alignment of different materials, heterostructures are designed to form variety of heterojunctions: (i) n-n heterojunction to fabricate photoanode in which the CB of the material exposed to electrolyte should be higher than that of the other material, (ii) p-p heterojunction to form photocathode in which the CB of the material exposed to electrolyte should be lower than that of the other material (iii) p-n heterojunction can be used to form either photoanode or photocathode. These heterojunctions formation can lead to the better charge separation, improved light harvesting ability and better stability of the photoelectrode material. The main parameter that decides the feasibility of heterojunction is the band edge alignment between the two semiconductors. In turns, this alignment depends upon the band gap and the electron affinity of the semiconductors (Wang et al., 2013). Consequently, depending upon band alignments three different types of heterojunction structures can be formed i.e. type I, type II, and type III. In case of type I which is also called straddling gap alignment, the heterojunction is formed between wide band gap and small band gap semiconductors, followed by the fact that the CB and VB of the wide band gap

semiconductor should be more negative and more positive than that of small band gap semiconductor, respectively. Due to such alignment of the band positions, the photo-excited electrons and holes are transferred to the CB and VB of the small band gap semiconductor, respectively i.e. the flow of the charge carriers is in the same direction towards small band gap semiconductor (Afroz et al., 2018). The heterojunction formed between the TiO_2 and Fe_2O_3 is an example of such kind of band alignment. In staggered gap arrangement i.e. type II structure, the photoexcited electron and holes move in opposite direction because the CB and VB of the one material are both more negative than the CB and VB of the other material, respectively. Such Kind of heterostructure is illustrated by most popular combination i.e. $BiVO_4$ and WO_3. The type III structure which is also popular by name 'broken gap' is almost similar with that of type II structure, but the difference lies in the fact that there is no overlapping of the bands because both CB and VB of the one material (say A) are more negative by the CB of the other material (say B). Therefore, the electron from the CB of the material B neutralized with the holes in the VB of the material A, and the electrons in CB of material A and holes in the VB of the material B carry out the redox reaction with water. An example of such kind of arrangement is heterojunction between FeS_2 and Sb_2Se_3 (Moniz et al., 2015). Besides the morphology and band alignment, one more parameter should also be considered while selecting the materials for heterostructure architecture, that parameter is the 'lattice mismatching' due to the difference in the lattice spacing of the two materials. This lattice mismatching becomes the reason for the creation of the enhanced interfacial defects, and as a consequence of this, electron-hole recombination is increased and also the band alignment structure is altered at the interface (Djurišić et al., 2020). So, low lattice mismatching between the two materials is suggested for heterostructure formation. Among all the aforementioned structures of the heterojunctions, the staggered alignment is one of the most effective one because the bend bending caused by the potential difference between the two materials creates a build-in electric field, which allows the photoexcitons to move in opposite direction leading to the most effective segregation of the charge carriers. The type II structure is also included into the Z scheme designing of the materials to form photoelectrode. The Z scheme design consists of same staggered alignment of the bands, but in this, alike type II heterojunction the electrons from the CB o the one material goes to the VB of the another material through an electron mediator (such as

Fe^{3+}/Fe^{2+}, IO_3^-/I^- and NO_3^-/NO_2^-. A variety of such Z-scheme photocatalysts have been reported in the literature in the field of photocatalytic water splitting and degradation of pollutants, but recently, this approach is also introduced in the field of photoelectrochemical water splitting. For example, Pan and his fellows has demonstrated a Z-scheme PEC cell consisting $Cu_2O|RuO_x$ as a photocathode and $BiVO_4|Mo$ as a photoanode. This cell provided bias free PEC water splitting (Pan et al., 2018). Another example of z scheme implementation in photoelectrochemical cell comes from the work of Wen and his cowokers in 2020, they has fabricated a very unique design of photocathode i.e. 3D z scheme urchin like structure of ZnO/Au/g-C_3N_4, in this Au NPs acted as the electron transfer mediator in the heterojunction between ZnO and gC_3N_4. This design provided a way for the forthcoming research to design z scheme based PEC cell (Wen et al., 2020). Also recently, Zheng et al reported advantage of the z scheme heterojunction over traditional type II heterojunction in designing photoelectrodes for photoelectrochemical water splitting cell. They demonstrated bias-free PEC water splitting with WO_3/Cu_2O direct z scheme heterojunction under visible light illumination, while WO_3/Cu_2O type II heterojunction provided water splitting under applied external potential (Zheng et al., 2020). Likewise, Zhou et al traced the construction of bird-like ZnO/TiO_2 photoanode based on z scheme heterojunction, which provided the improved performance in terms of photoelectrochemical water splitting (Zhou et al., 2020). The introduction of this z scheme heterojunction in photoelectrochemical water splitting is emerging as an innovative idea, as this Z scheme approach for photocatalyst is among the most promising one, especially when it is used with the some other modifications like plasmonic material decoration.

5. Different ways the metal nanoparticles induced surface modifications may influence the process

The motivation for using plasmonic nanostructures to PEC water splitting came largely from the facts that were discussed by Warren et al (2012) in their review article. They highlighted the problems that a photoelecrode designing approach is facing and suggested the role of plasmonic metals to surmount them. These problems are: (i) Short minority carrier distance for most of the semiconductors leading to the recombination of photo-excited charge carriers at the bulk of the semiconductor, by the incorporation of the plasmonic metal nanoparticles alternative location for electron hole pair formation

can be provided (ii) The challenge of designing cost-effective photoelectrode with high absorption coefficient can be fulfilled by using plasmonic nanoparticles, as in small size they act as antennas to harvest maximum light from solar spectrum while large size nanoparticles can make use of scattered light. (iii) To deal with low STH conversion efficiency of wide bandgap semiconductors, plasmonic metal can play critical role by acting as sensitizer (iv) High refractive index of many semiconductors loose energy by reflection of light surfaces, by the use of plasmonic metal nanoparticles detraction in reflection can be achieved to a nearly negligible level (v) Plasmonic metal nanostructure can be used to reduce interfacial area between semiconductor and electrolyte, which can help in increasing photo-potentials. Actually, plasmon-assisted metallic nanoparticles show a unique resonance phenomenon, which is known as Surface Plasmon Resonance. Under electromagnetic light illumination, the electrons present on the surface of the metal start collective oscillations, and when the oscillating frequency of these electrons matches with the incident light frequency, at this condition, SPR phenomenon occurs. This SPR effect of metals can broadly be classified into two mechanisms: (i) SPP (Surface Plasmon Polariton), and (ii) LSPR (Localized Surface Plasmon Resonance). The Surface Plasmon Polariton involves the propagation of the electromagnetic wave at the interface of metal and dielectric medium, resulted by the resonant oscillations of electrons, and it occurs for bulk metal surfaces such as films. In contrast to this, LSPR effect is shown by metal nanoparticles or nanostructure, owing to their small sizes, this mechanism also involves the excitation of surface electrons through collective oscillation under incident light illumination, but this mechanism to generate plasmons is regionally limited or confined to nanoparticles surface only. After the excitation of the surface electrons to form plasmons, the de-excitation or damping mechanism for plasmons take place. In real sense, these LSPR damping mechanisms are responsible for the enhancement in the photolectrochemical water splitting. Basically, there are three mechanism through which a plasmon can relax: (i) Near-field electromagnetic enhancement mechanism (PIRET), (ii) Hot electron injection mechanism, (iii) Light scattering mechanism. These mechanisms explain reasons behind the enhancement in the performances.

(i) Near field electromagnetic enhancement mechanism or (PIRET)

(ii) In this mechanism, the strong electromagnetic field is created by plasmons due oscillation of electrons on the surface of metal nanostructure, and when the semiconductor comes in close proximity of these metal nanostructures, it experiences the enhanced electromagnetic field, which cause the more excitation of electrons in the semiconductor to generate more photo-excitons, thereby help in increasing the carrier density. The same increase in carrier density i.e more generation of photo-excitons lead to one another mechanism caused due to this enhanced electromagnetic field, which is known as Plasmon-induced resonance energy transfer (PIRET). PIRET take place when the Plasmon non-radiatively damps its energy to relax itself through dipole-dipole coupling. This damped energy can be transferred to the semiconductor to generate electron-hole pair, when it is absorbed by it. Mostly, this transfer is possible when the bandgap of the semiconductor is lower than the near field energy, but some reports have shown that it is possible when band gap is higher (Atabaev et al., 2018). This mechanism is highly depended on the resonant frequency of the plasmons, distance between the semiconductor and metal, and absorption extinction of semiconductor and overlapping of absorption spectra. And overall, this near field enhancement help in reduction the recombination rate of charge carriers.

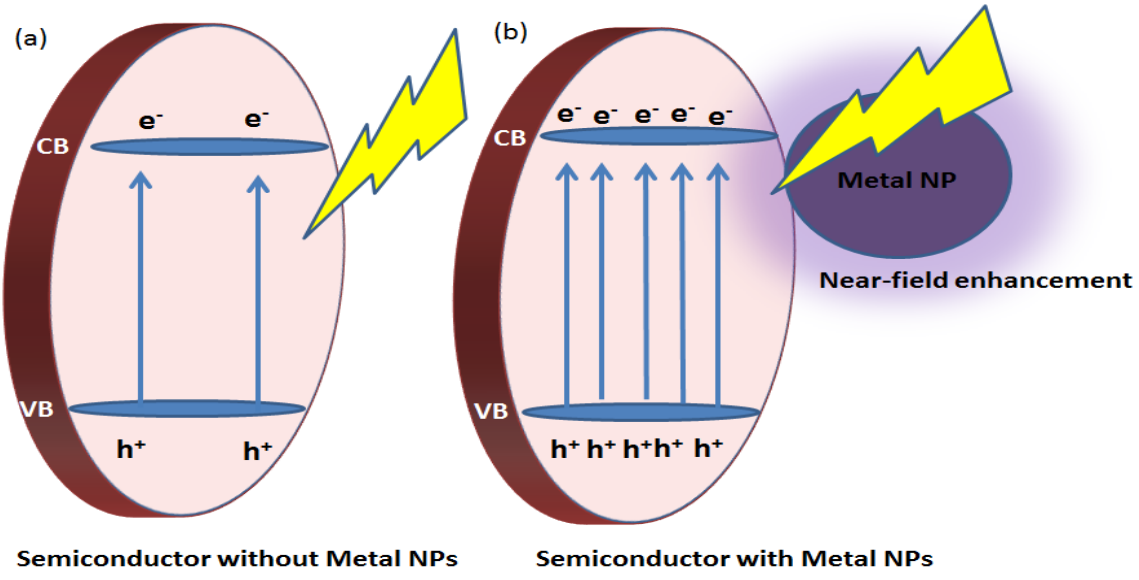

Fig. 2 (a) Generation of electron hole pair in absence of metal nanoaprticles, (b) Increase in the electron hole pair generation due to the near-field enhancement caused by the decaying of LSPR of metal NPs.

(iii) Light scattering and light concentration mechanism

Light scattering mechanism of plasmonic nanostructure is dependent on the light scattering-to-absorption ratios, which are in turn depend upon the size of the metal nanostructure, and it is observed that the larger size particles show prominent light scattering effects. Moreover, the shape and geometry of metal nanostructure can also influence the scattering phenomenon, nanocubes shows better scattering than nanowire and nanostars, thereby greatly improves PEC performances. In this mechanism, the plasmon release energy radiatively in the form of photons, and then, these photons are subsequently absorbed by the other metal nanostructures. As a result of this, average path length of the incident photons is increased and also the maximum utilization of the incident light is possible by taking the advantage of the unused photons (Christopher et al., 2010). In this way, light scattering mechanism helps in generation of more electron hole pairs that can participate in water splitting redox reactions.

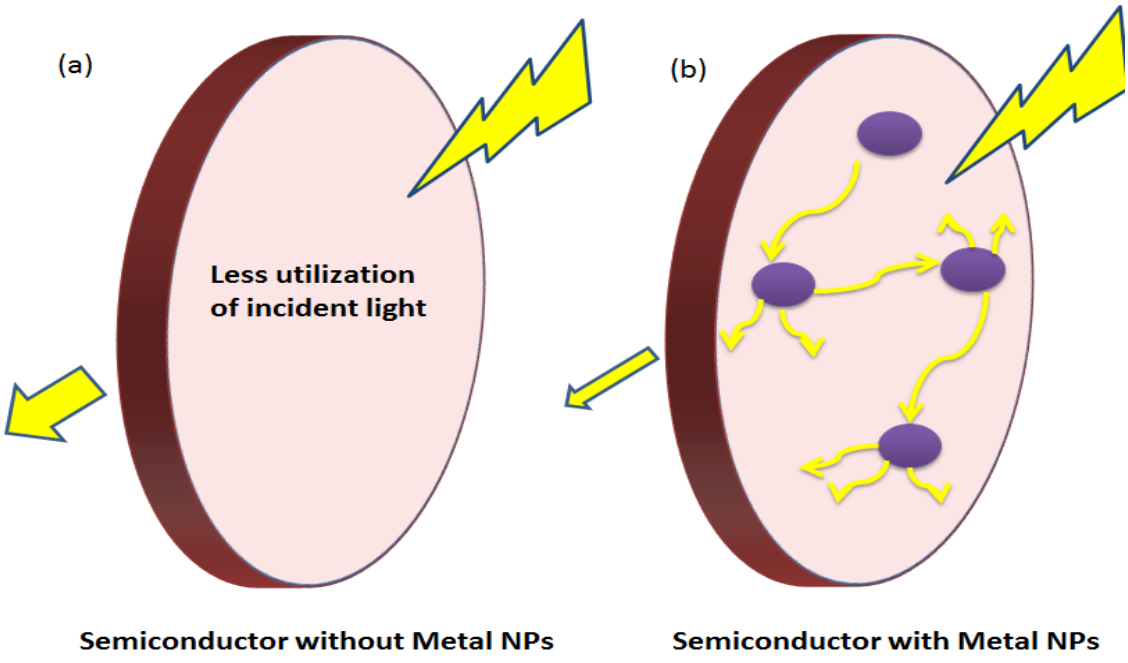

Fig. 3 (a) Incident light is less absorbed or more transmitted by the semiconductor in absence of metal NPs, (b) The decaying process of LSPR of metal NPs by light scattering make more use of incident light by increasing the averge path distance of incident light.

(iv) Hot electron injection mechanism

When the decay of LSPR effect of plasmons doesn't take place by the above mentioned two mechanisms i.e. neither by the light scattering nor by the near field electromagnetic enhancement mechanism, then, the plasmonic energy is absorb by the metal nanostructures to generate higher

energy electrons and holes i.e. hot electrons and holes. This is referred as non-radiative decay of plasmons. These hot electrons make metal nanostructure to behave as photosensitizer and enable the use of visible as well as some near IR light. In metal nanostructures or nanoparticles, plasmonic charges lie at the Fermi energy level as the concept of homo-lumo or valence band-conduction band don't exist. This hot electron injection mechanism can be influenced by various factors such as size, shape, loading amount, and the intrinsic characterstics of the semiconductor along with interfacial conditions between semiconductor and metal. This mechanism is dominant for smaller nanoparticles. Hot electron injection can be done in two distinct mechanisms i.e. indirect mechanism and direct mechanism. In indirect mechanism, first the generation of hot electrons by plasmon decay, then these hot electrons reached to the interface and only those electrons which have higher energy than the schottky barrier are injected into the conduction band of the semiconductor. In case of direct mechanism, hot electrons are directly injected into the conduction band of semiconductor without any intermediary step. This process involve chemical interface damping (CID) i.e. new hybridized electronic states are incorporated about the Fermi level of the metal at the metal semiconductor interface. Direct mechanism is much better than the indirect mechanism owing to the faster rate of LSPR relaxation and non-thermal decaying nature (Lee et al., 2017). But direct injection mechanism is recently emerging explanation and much more exploration is required.

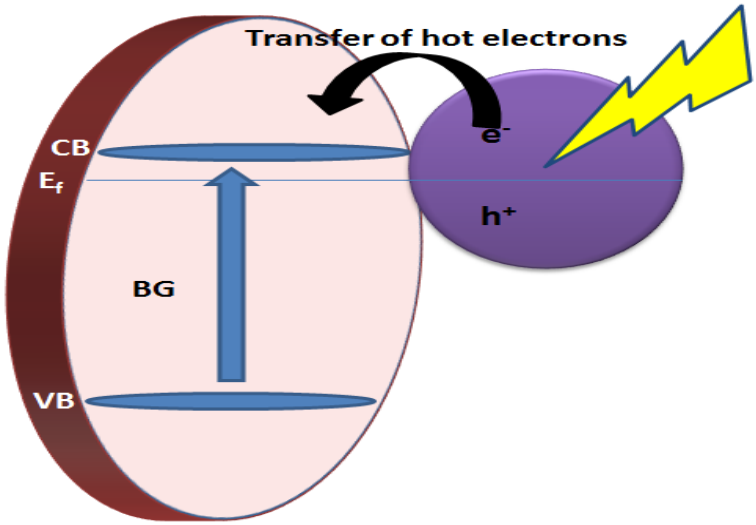

Fig. 4 Hot electron injection mechanism of LSPR decaying of the metal NPs leading to the transfer of the electrons to the conduction band of the semiconductor.

Metals that show plasmonic effects can broadly place under the two categories i.e. noble metals and non- noble metals. For PEC-oriented applications, plasmonic metals should have properties like cost-effectiveness, stability in electrolyte, long lifetime, and good catalytic properties. Noble metals include Au, Ag, Cu, Pd, Pt and Ni and non-noble metals have in line Al, Bi, transition metal nitrides such as TiN and ZrN, and metal dichalcogenides (MXenes). However, intensive research has been done on Au and Ag because of their plasmonic effect with high stability, but these metals are in general costly in nature and only suitable for understanding the fundamentals of plasmonic effect on PEC water splitting as they have no practical future. So, in search cost effective plasmonic metals Cu and Al came into the picture, but in case of Cu and Al, there is a problem of chemical stability. Additionally, noble metals are not suitable for the complementary metal oxide semiconductor devices (Mascaretti et al., 2019). The use of non-noble metals is drawing much attention these days to surmount the issues associated with noble metals. Transition metal nitrides and dichalcogenides are new developing materials.

Since last one decade, plasmonic-assisted PEC water splitting is investigated with great interest. There are several unique configurations in which a plasmonic metal can be used to design a photoelectrode such as they can be deposited beneath the semiconductor, on the surface of the semiconductor and can be sandwiched in between the two semiconductors. The coupling interaction between incident light and surface plasmons can be enhanced the electromagnetic field and provide better PEC response of WO_3, when Ag NPs of size 10-50 nm embedded beneath WO_3 semiconductor (Solarska et al 2012). The different loading amount of Ag NPs leads to the different effect on the PEC performance. The optimized the loading amount of Ag NPs on the surface of WO_3 to make maximum use of SPR effect of Ag NPs (Naseri et al., 2013). The sandwiched configuration was designed in the literature by preparing Au/TiO_2/Au photoanode, this configuration provided better efficacy than single decoration (Li et al., 2013). The different sizes of plasmonic metal have positive or negative effect on PEC performance (Chen et al., 2013). As the size of the Ag NPs increased after an optimum value on the surface of TiO_2, then, the negative effect on the PEC performance was observed. After this, a new approach of using plasmonic metals in combination with heteronanostructure and other modifications

has been started. Guo et al (2015) synthesized photoanode TiO_2/Ag/Ag_2S/Ag_3CuS_2 NRs. SPR effect along with sensitization with binary and ternary sulfide helped in increasing light absorption and charge separation leading to enhanced performance. Zhang et al (2016) prepared two-story heteronanostructured photoanode with the use of plasmonic metal decoration on both stories. Au-decroated CdSe@rGO(upper story)+ Au decorated CdSe@ZnO (bottom story). This unique design has provided highest photocurrent density of 10mA/cm^2 at 0 V vs SHE. Recently, the use of plasmonic metal other than Au and Ag is gaining interest. The use of Al as a plasmonic metal was shown by Chen et al (2020) by preparing a highly efficient Al/Cu_2O/NiS photocathode. Subramanyam and his cowokers (2020) combined Cu NPs with Bi_2S_3 QDs to decorate WO_3 and provide high PEC performances. Bi NPs are showing great potential for replacing noble metals (Wang et al., 2017, Subramanyam et al., 2010).

6. Proposed Study: Genesis

The genesis of the proposed work lies in the ongoing hunt for a suitable material/material system that can be used as efficient photoelectrode to achieve PEC hydrogen generation. The success here rests upon meeting the multiple technical challenges related to synthesizing new and efficient materials/material systems (semiconductors) with desired properties and their thorough characterization. The most widely investigated class of materials in this reference is oxides of metals with d^0 and d^{10} configuration. Several metal oxides have been explored in the past for their possible use in PEC water splitting. Yet, none are able to meet all the properties required. The phenomenon of PEC water splitting proceeds through three broad steps: (a) photogeneration of charge carriers on the exposure of solar radiation, (b) migration of charge carriers to surface without recombination and (c) reduction and oxidation processes for the production of hydrogen and oxygen via splitting of water. While, the first two steps depend on the structural and electronic properties of materials used, the third and probably the most crucial step depends majorly on the semiconductor-electrolyte junction characteristics. It is now largely established that the surface properties of semiconductor electrode play a vital role in facilitating or otherwise of the whole process. In this reference, recent studies have indicated that the effects generated by surface plasmonic resonance of metal nanoparticles can yield critical breakthrough.

From the literature survey undertaken (Please see Annexure), it is apparent that there exists an important domain of fundamental research, where working with different semiconductor nano-hetero-strucutres, the effects of metal-SPR induced surface modifications on PEC performances of the electrodes still need to be investigated in greater detail. Further, in recent years when the thrust is more on combining the advantages of more than one material and to generate a better and more efficient material system for PEC water splitting, the role and significance of nano-hetero-structures has assumed tremendous significance. In this reference, few of the promising materials for application in PEC water splitting are listed in Table 1.

Table 1: Few promising materials for application as photoelectrode in PEC water splitting.

Materials	Band gap	CB edge	VB edge	Remarks
$NaNbO_3$	3.30	-0.68	2.62	• n-type, favorable band edge positions, direct bandgap • ferroelectric characteristic at room temperature • piezoelectric material • direct replacement of ZnO and TiO_2 • non-toxic, low cost, good corrosion resistant • chemically stable (stable in aqueous solutions) • high carrier mobility (in comparison with other ferroelectric materials like $BaTiO_3$) **Limitations** • wide band gap • fast recombination
$SrTiO_3$	3.30	-1.32	2.02	• high chemical stability • favorable band edges • non-toxic, low-cost, environment-friendly, stable against corrosion and photo-corrosion **Limitations** • Large bandgap • Rapid recombination rate *Heterojunction formation with suitable narrow bandgap materials and plasmonic metal sensitization might prove beneficial for PEC water splitting.*
Co_3O_4	2.07	0.30	2.44	• p-type, non-toxic, low cost • finds use in water electrolysis for OER owing to its high catalytic behavior for water splitting • highly stable in aqueous alkaline environment **Limitations**

				• slow separation of photo-induced electron-hole pairs
$InVO_4$	2.11	-0.5	1.5	• n-type, stable, proper band alignment, • visible light absorption
gC_3N_4	2.7	-1.22	1.5	• 2D-structured metal-free semiconductor • polymeric semiconductor • suitable band edges for water splitting • nontoxic, low cost, simple fabrication, and high physicochemical stability **Limitations** • high recombination rate, poor electronic conductivity, sluggish hole-transfer, • limited visible light absorption at long wavelength range of 460 to 760 nm
Bi_2S_3	1.39	0.9	1.48	• n-type, low cost • narrow band gap can be used for heterojunction formation
Sb_2Se_3	1.2	-3.98 (vacuum)	-5.19 (vacuum)	• p-type, non toxic, earth-abundant, low cost • can be used as narrow band gap semiconductor in heterostructure formation • attractive optoelectronic properties and high mobility • Sb_2Se_3 is intrinsically stable towards photocorrosion in strong acidic media unlike Cu_2O
BCN	Tunable, depending on N and C content			• Graphene, the single atomic layer of carbons expresses a zero bandgap, whereas the h-BN possesses a wide bandgap (5.5 eV). Both materials are therefore not suitable as photocatalyst. However, intermediates of these layered materials (called ternary BCN compounds) could constitute the desired medium-bandgap semiconductors where bandgap and absolute energy levels can be adjusted by chemical variations. • Stable • Can be used as visible light driven photocatalyst • Suitable to make heterojunction

7. Proposed study: Definition

Systematic explorations on combining few of the most promising semiconductors to obtain bilayered nano-hetero-structured thin films, which will be subjected to metal nanoparticles-induced surface modifications (viz. surface plasmon resonance) to evolve efficient photoelectrodes for PEC water splitting. The goal here would be to synthesize bi-layered nano-hetero-structureed thin films on ITO glass substrate, where the top layer would be surface modified either during or post film deposition.

The films, thus obtained, would be subjected to thorough characterization for their use in PEC water splitting.

8. Objectives/Stages of the Proposed Work

The main objectives/stages of the proposed work are listed below:

- Synthesis of metal (Ag and Au) nanoparticles through controlled reduction via biological/chemical routes.
- Synthesis of bi-layered thin film nano-hetero-structures of chosen semiconductors by wet chemical routes, viz. sol-gel spin coating/spray pyrolysis, and the surface modifications induced by metal-SPR.
- The characterization of films for crystallographic, morphological and other semiconductor properties relevant to PEC water splitting.
- PEC water splitting studies using the films prepared as working electrode and measurement of the performance indicating parameters.

9. Proposed Methodology

Metal nanoparticles will be prepared from their low-cost compounds via controlled reduction in an aqueous system by chemical/biological routes. In the biological route, appropriate biological (plant derived) materials, viz. spirulina (algae), tea and other plant extracts etc would be employed. Conducting glass plates will be used as substrate for film deposition. Films would be prepared by sol-gel spin coating and/or spray pyrolysis. Sintering at high temperature would enable the evolution and growth of the desired crystalline phase. In the top few layers of the films, metal nanoparticles would be embedded during the course of films synthesis or post-synthesis. After systematic and thorough characterization of films, these would be subjected to PEC studies.

10. Tentative Plan of the Work

A tentative plan of proposed work and the parameters/variables of investigation have been outlined below:

Table 1: Tentative plan of the proposed work

Parameters of the study	Description
Preparation of samples Materials of interest	Few of the following: First generation materials: ZnO, α-Fe_2O_3, CuO Second generation materials: $NaNbO_3$, $SrTiO_3$
Proposed avenues for investigation	▪ Bilayered nano-hetero-structures (Thin films) ▪ Surface modifications induced by metal (Ag, Au) nanoparticles-SPR
Proposed methods for sample synthesis	Wet chemical processes (Sol-gel and spray pyrolysis).
Expected variables in the study	*Preparation of samples* ▪ Nature of metal oxides and their combinations ▪ Sintering Conditions: Temperature, Environment ▪ Metal nanoparticles
Material characterization	▪ Phase identification and microstructure by XRD analysis ▪ Surface morphology by SEM analysis ▪ Surface topography by AFM analysis ▪ Elemental composition and stotichiometry by EDX and XPS analyses ▪ Band gap energy by UV-Visible spectrometry ▪ TEM analysis of selected high-performing samples ▪ Film thickness by surface profilometer ▪ Density ▪ Elctrical resistivity ▪ Flatband potential and carrier density
PEC measurement variables	▪ Current-Voltage characteristics of the PEC cell under darkness and illumination. ▪ Photovoltage and Photocurrent ▪ Open circuit potential ▪ Short circuit current ▪ Onset voltage ▪ Applied bias photon to current conversion efficiency (ABPE)

Literature review in the proposed area of work

Kumar et al (2021) prepared Ag/$NaNbO_3$ photoanode through hydrothermal and chemical solution method followed by spray coating technique used for fabrication. The synergistic effect of plasmonic metal and piezoelectric semiconducting material was investigated on the photoelectrochemical studies and photocatalytic studies. The Ag/$NaNbO_3$ photoanode exhibited a photocurrent density of 9.56mA/cm^2 at 1 V vs Ag/AgCl under ultrasonic vibrations and light illumination. This was almost 9-fold enhancement compared to bare $NaNbO_3$ without plasmonic metal and ultrasonic vibrations. The overall improvement in PEC performance was ascribed to the plasmonic and piezo-phototronic effect of this combination. The SPR mediated hot electron injection improving the visible light absorption

and the built-in electric field by piezo-phototronic effect enhanced the charge separation efficiency through more upward bend bending resulting in the proper band alignment.

Celebi et al (2021) successfully prepared Au/TiO2 photoelectrode with simple and cost effective synthetic approach without ligand assisted process. The simple binding approach was applied and only small quantity Au nanoparticles are attached to form schottky contact. The performance of the as-synthesized photoelectrode was showing enhanced performance as compare to the bare TiO2. The photocurrent density of 1.87mA/cm2 was obtained at 0.187V vs RHE. The improved performance was attributed to the SPR effect of Au NPs leading to the effective charge separation and low recombination.

Huynh et al (2020) fabricated Cu-doped ZnO NRs decorated with Au NPs. The change in the optoelectronic properties with Cu doping concentration was tested. At low concentration of Cu doping (3%), band gap of ZnO NRs narrowed down to 3.09 eV allowing absorbance towards red light. Au NPs (approximate 10 nm) were decorated on ZnO:Cu NRs using thermal evaporator. The PEC performance was improved with photocurrent density of 10.2μA/cm² at 0.581 V (approx. 7.3 times higher than pristine ZnO NRs) under visible light irradiation (λ>420 nm). The maximum STH conversion efficiency came out to be 0.59%. The SPR effect of Au NPs and injection of hot electrons into the CB of NRs enhance the absorbance in visible region, and suppress the charge recombination, also the synergetic effect of Cu dopant and Au Plasmon helped in minimizing recombination and increase the photocatalytic activity.

Ghobadi et al (2020) successfully designed a large scale compatible fabrication of Au-capped TiO_2 NWs using shadowing effect of NWs. The TiO_2 NWs were prepared via hydrothermal method and AuNPs were deposited by angle via angle deposition technique. This visible light driven photoanode was showing a photocurrent density of 82μA/cm^2 0.62 V vs Ag/AgCl. This better performance was originated from hot electron injection and near field effect of the plasmonic Au nanocaps. This architecture was showing photostability of 2h.

Zheng et al (2020) fabricated plasmonic metal/semiconductor with inverse opal structure (Au/ZnO-IO) via simple template method, by which AuNps were in-situ grown on the ZnO-IO to form heterojunction. This nano-composite show superior PEC performance of 0.6mA/cm^2 at 0.6 V vs

Ag/AgCl than Au/ZnO-P and ZnO-IO. The enhanced photocatalytic activities were attributed to the increased light trapping and special transfer of carriers from Au NPs to ZnO and then ZnO to another Au particle, which significantly helped in charge separation efficiency.

Gao et al (2020) modified TiO_2 nanorods with AgNPs and Al_2O_3 passivation layer to form Al_2O_3/Ag/TiO_2 nanorod photoanode via hydrothermal, magnetron sputtering and ALD methods. UV-vis absorption spectra, PL spectra and transient photocurrent response showed that after deposition of the AgNPs on TNRs light absorption increased, separation and reduction in recombination rate enhanced and concentration of photoexcited carriers increased by hot electron injection (LSPR effect). The Ag/TNRs photoanode had a photocurrent density of 0.056mA/cm^2 at 0 V vs. Ag/AgCl (5 times than pure TNRs). Moreover, the photocurrent density was increased to 0.34mA/cm^2 by the passivation of ultra thin layer of Al_2O_3, which decrease the density of the surface defects.

Cui et al (2020) successfully synthesized the Ag/NH_2-MIL-125/TiO_2 hybrid photoanode by simple hydrothermal reaction and soaking process (reduction process). The PEC study showed that photocurrent density had been increased to 1.06mA/cm^2 at 1.23 V vs. RHE. Highest IPCE of 51.0% had been obtained which was almost 2-fold higher than bare TiO2. The PEC stability for 3 h under constant illumination had been also achieved. After decorating AgNPs to MOF/TiO_2, there was negative shift in the onset potential of the photoanode and this shift was ascribed to the formation of schottky barrier between AgNPs and TiO_2 reducing the charge recombination. This was attributed to the synergetic effect between MOF and Ag NPs which included effective separation of charge carriers, enhanced light-harvesting capacity, improved water oxidation kinetics and increased photoanode overall conductivity.

Chen et al (2020) had prepared a cost effective and highly efficient Al/Cu_2O/NiS ternary photocathode by simple magnetron sputtering, electrodeposition and SILAR methods. Al NPs with SPR effect provided the hot electron injection to the conduction band of Cu_2O NCs enhancing the local electromagnetic field. Meanwhile, the electron trapper NiS NPs rapidly captured the electrons transferred from the conduction band of Cu_2O NCs which reduced the recombination of the charge carriers. Therefore, the integration of Al and NiS on the Cu_2O NCs was conducive to boost the absorption of light and to elevate transfer and separation of charge carriers. Al/ Cu_2O /NiS hybrid

membrane showed a photocurrent density of -5.16mA/cm² at 0V vs. RHE (eight-fold increment than Cu_2O).

Subramanyam et al (2020) had successfully designed $WO_3/Cu/Bi_2S_3$ photoanode via hydrothermal, electrophoresis and SILAR methods. The as-synthesized photoanode had a photocurrent density and STH conversion efficiency of 10.6mA/cm^2 at 1.23 V vs. RHE and 3.21% at 0.81 V vs. RHE (higher than WO_3/Bi_2S_3 and bare WO_3). Absorption spectra and PL spectra showed that after Cu NPs incorporation to WO_3/Bi_2S_3 there was enhancement of light absorption showing that good interfacial contact is formed between Cu NPs and semiconductor for efficient light harvesting, low charge transfer resistance and also there was suppression of recombination of carriers. Moreover, LSV curves taken for 50 cycles showed that photocurrent density retained without decay in PEC performance indicating that Cu NPs also increased the photochemical stability of the photoanode. Also, highest IPCE of 51% was achieved.

Han et al (2020) prepared Cu@ZnO NWs photoanode via two-step chemical vapor deposition and magnetron sputtering methods. The structural and optical properties of this photoanode were investigated at different sputtering time (ST) and sputtering power (SP). The morphological analysis showed that size and amount of Cu on ZnO was optimized by controlling ST and SP. ST and SP controlled the thickness and average diameter of Cu nanostructures, respectively. Cu@ZnO NWs exhibited highest photocurrent density (5.2μA/cm^2 at 1 V vs. Ag/Agcl) at SP of 5 W and ST of 80 s, which is higher than the bare ZnO NWs (4.0μA/cm^2). At this composition, SPR-effect of Cu Enhanced the PEC performance. At higher SP the photocurrent density decreased as large coverage of ZnO NWs by Cu NPs hindered the absorption of light.

Subramanyam et al (2020) had prepared Bi NPs decorated $rGO/BiVO_4$ photoanode via chemical reduction, Hummer's method and drop casting method. The photocurrent density of bare $BiVO_4$ was 2.39mA/cm^2 at 1.23 v vs. Ag/AgCl, this value was increased to 3.56 mA/cm^2 by decoration of the Bi NPs, which was further reached to 6.05 mA/cm^2 at the same bias under visible light illumination. The enhanced photocurrent density was attributed to the increased visible light absorption, efficient charge separation and transfer by SPR of Bi iNPs and increased carrier density by hot electron injection. The

rGO nanosheet played very important role increasing carrier transfer owing to its great conductivity and providing chemical stability to the photonode confirmed by chronoamperometric measurements.

Li et al (2020) fabricated a photocathode consisting of Pt nanoparticles decorated on TiO_2 nanoballs via photoreduction method, then deposited over CdS/Cu_2ZnSnS_4 heterojunction via spin coating method. The resulted photocathode was designated as Pt/TiO_2-NB/CdS/CZTS. This modification of TiO_2 NB was done to replace traditional and expensive ALD TiO_2 passivation layer and to provide comparatively more advantageous properties such as high specific area, low preparation cost, controllable size, homogeneously distribution of Pt nanoparticles on its surface. The size of Pt_{nps} and thickness of Pt_{np}/TiO_2 NB layer were optimized to get highest PEC performance. To investigate the SPR effect of Pt_{nps} the FDTD theoretical simulations were done. The near electric field enhancement was there, not only on the surface of the Pt_{np}/TiO_2 NB layer but also inside the Pt_{np}/TiO_2 NB layer influencing CdS/CZTS heterojunction's electric field. As the result of these effects the charge separation efficiency improved, transfer of the charge carriers at interface improved, and charge carrier lifetime increased. The as prepared photocathode showed a best photocurrent density of 17.2 mA/cm^2, V_{OC} of 0.7 V_{RHE} and half cell-solar to hydrogen efficiency of 3.5%.

Kumar et al (2021) prepared Ag/$NaNbO_3$ photoanode through hydrothermal and chemical solution method followed by spray coating technique used for fabrication. The synergistic effect of plasmonic metal and piezoelectric semiconducting material was investigated on the photoelectrochemical studies and photocatalytic studies. The Ag/$NaNbO_3$ photoanode exhibited a photocurrent density of 9.56mA/cm^2 at 1 V vs Ag/AgCl under ultrasonic vibrations and light illumination. This was almost 9-fold enhancement compared to bare $NaNbO_3$ without plasmonic metal and ultrasonic vibrations. The overall improvement in PEC performance was ascribed to the plasmonic and piezo-phototronic effect of this combination. The SPR mediated hot electron injection improving the visible light absorption and the built-in electric field by piezo-phototronic effect enhanced the charge separation efficiency through more upward bend bending resulting in the proper band alignment.

Huang et al (2020) prepared $CoO_x/BiVO_4$ photoanode by using an easy impregnation and calcination method, and cobalt oxide was loaded as nanoparticles. The resulted photoanode was showing the photocurrent density of 3.1mA/cm^2 at 1.23 V_{RHE}, which was almost 2.8 times than that of obtained by

using bare $BiVO_4$, and negatively shifted onset potential was obtained for water oxidation. Here, Cobalt oxide acted as water oxidation co-catalyst to improve the kinetics of OER and it also formed the p-n heterojunction with $BiVO_4$, which was responsible for better charge separation and injection efficiency to about 90% and & 70%. The formation of p-n heterojunction was verified by using input voltage-output current characteristic curve.

Wen et al (2020) designed three dimensional (3D) z scheme urchin-like ZnO/Au/g-C_3N_4 photocathode. The photoelectrode was fabricated by drop casting method. This unique z scheme arrangement exhibited a consistent photocurrent density of -0.2mA/cm^2 for almost 10 hrs at 0 V_{RHE} in the presence of Pt as co-catalysts. In this heterostructure, Au nanoparticles acted as electron mediator between ZnO/g-C_3N_4 heterojunction, which led to vectorial transfer of electron from the CB of ZnO to the VB of g-C_3N_4. In addition, heterojunction formation provided better light absorption in the visible region and improved charge separation. The 3D urchin-like structure facilitated path-directed transfer of the charge carriers.

Zheng et al (2020) fabricated WO_3/Cu_2O photoelelctrode based on direct z scheme heterojunction formation. The fabrication was done by using seed-mediated hydrothermal method followed by the electrodeposition technique. The design was optimized by the controlling electrodepositing amount of the Cu_2O. The photoelectrode WO_3/Cu_2O-30 min provided the enhanced PEC performance than the individually used WO_3 and Cu_2O. This optimized photoelectrode exhibited bias free PEC water splitting and showed a photocurrent density of 12μA/cm^2 in the visible light illumination. The corrosion of the Cu_2O was restricted by this z scheme heterojunction formation as the holes generated in its VB were neutralized by the electrons from the CB of the WO_3. At the same time, the electrons and holes in the CB of Cu_2O and VB of WO_3 were freely available for the participation in the water redox reactions.

Zhou et al (2020) had fabricated two different heterostructure of the ZnO/TiO_2 direct z scheme heterojunction to design photoelectrode i.e. bird nest (BN) ZnO/TiO_2 and sealed core shell (CS) ZnO/TiO_2 heterostructure. The synthesis was done by simple hydrothermal method and spin coating technique, and the dispersion and loading amount of ZnO was controlled by the spin coating speed. In comparison to the CS, the BN heterostructure provided enhanced PEC performance with photocurrent

density of 2.75mA/cm^2 at 1.23 V_{RHE} (1.38 times than CS heterostructure). The stability of BN heterostructure was also better than that of CS over 8 hrs of continuous light illumination. The improvement in the PEC performance was due to the better charge separation owing to the direct z scheme band alignment of heterojunction. Meanwhile, the bird nest structure provided enhanced light harvesting and improved charge carrier kinetics.

Esmaeili-Zare et al (2020) had prepared $CuInS_2$/CdS/ZnO/ZnO:Al/Au photocathode by using electrodeposition, chemical bath deposition, and magnetron sputtering methods. The effect of pH and concentration of the electrolyte on the photocurrent density of this photoanode was also monitored. The as synthesized photocathode showed highest photocurrent density of -1.91mA/cm^2 at -0.6 $V_{Ag/Agcl}$ and pH=8. The p-n heterojunction formed by the layer of CdS over CIS helped in improving the charge separation efficiency and inhibited the recombination of charges at the interfaces. ZnO restricted the back flow of electrons owing to wide bandgap of it and it also helped in the efficient transfer of the charge carriers.

Jiang et al (2020) had fabricated PbS quantum dot sensitized ZnO nanorod/$ZnFe_2O_4$ nanosheet core/shell nanoarray photoanode. The methods used for its preparation were solvothermal, dip-coating technique and SILAR. The one dimensional architecture of the core shell heterostructure provided better direct transport and transfer of the photogenerated charge carriers. The formation of the heterojunction also enhanced the charge separation efficiency and light absorption efficiency. In addition to this, the anchoring by the PbS quantum dots extended the absorption of the photoanode in the visible region. The aforementioned advantages enabled the photoanode to exhibit the high photoelectrochemical performance, and the corresponding photocurrent density was reported as 0.577mA/cm^2 at 0.6 V_{RHE}.

Bai et al (2020) had fabricated reduced graphene oxide anchored SnO_2/$BiVO_4$ photoanode. This photoanode was obtained by deposition of SnO_2 on FTO using chemical vapor deposition method followed by the decoration of the $BiVO_4$ nanoparticles on to its surface using metal organic decomposition method, and finally, the rGO was spin coated over it. The resulted optimized photoanode showed an enhanced photocurrent density of the 2.05mA/cm^2 at 1.23 V vs RHE. The formation of the type II n-n heterojunction between SnO_2 and $BiVO_4$ aided the photoanode with high

charge separation efficiency and better light absorption especially in the visible region. The problem of the accumulation of charge carriers due to built in electric field of n-n heterojunction was tried to solve by the use reduced graphene oxide, which improved the conductivity of the photoanode.

Mu et al (2020) had successfully designed a photoelectrode SnO_2(0D)/SnS_2(2D) consisting 'Step Scheme' heterojunction. The photoelectrode was simply designed by using the solvothermal method and in-situ oxidation technique. The photoelectrode was optimized by controlling the annealing temperature. The optimized photoelectrode SnO_2/SnS_2-400 showed the highest photocurrent density of the 0.33mA/cm^2 at 1.23 V_{RHE}, and also exhibited the enhanced faradic efficiency. The reasons for such improved performance was the formation of the S Scheme heterojunction, helped in eliminating the electrons and holes having vulnerable capacity to take part in the water reduction-oxidation reaction by their recombination through this heterojunction and allowed the electrons and holes having strong capacity to participate in the water redox reaction. Therefore, the separation of the charges was efficient and also the light absorption was enhanced by this heterojunction formation.

Yaw et al (2020) had demonstrated the effect of anchoring rGO over the V_2O_5/$BiVO_4$ heterojunctioned photoelectrode. The photoanode V_2O_5/rGO/$BiVO_4$ was synthesized by elelctrodeposition and drop casting methods. The resultant photoanode was optimized by controlling the drop casting of the charge mediator layer of rGO and the highest photocurrent density of 2.1mA/cm^2 at 1.5 V vs. Ag/AgCl was obtained. The rGO interlayer between the type II staggered heterojunction led to the fast and efficient transfer of the photogenerated electrons therefore it acted as the electron mediator. The hydrogen evolution rate was found out to be 32.7 μmol/hr.

Guo et al (2020) had been successfully prepared TiO_2/$BiVO_4$ installed with Co-Pi cocatalyst nanoparticles. This photoelectrode was prepared by simple solvothermal and sol-gel methods. The photoelectrode showed a photocurrent density of 2.36mA/cm^2 at 1.23 V vs. RHE (9 times than that of pristine TiO_2). The type II heterojunction provided the extension of the light absorption edge into the visible region and also helped in the efficient charge separation. Meanwhile, the installation of the cocatalyst nanoparticles Co-Pi improved the charge transport dynamics of the photoelectrode as it act as the hole extractor.

Yaw et al (2020) had successfully anchored the heterojunction photoelectrode V_2O_5/rGO/$BiVO_4$ with the dual electrocatalyst NiOOH and FeOOH. The photoanode FTO/V_2O_5/rGO/$BiVO_4$/FeOOH/NiOOH was prepared by facile electrodeposition method. The photocurrent density obtained was 3.06mA/cm^2 at 1.5 V vs Ag/AgCl. Dual electrocatalyst incorporation limited the recombination of the surface charge carriers, which was not possible with the heterojunction alone. These electrocatalyst acted as the holes extractor to improve the interfacial charge transfer kinetics. The synergetic effect of the type II staggered heterojunction, electron mediator interlayer (rGO), and holes extractor electrocatalyst improved the overall PEC performance.

Xing et al (2020) had synthesized a ternary photoelectrode NiO/CuO/MoS_2 by easy hydrothermal and potentiostatic deposition method. In this design, CuO was sandwiched between dual co-catalyst NiO in bottom and MoS_2 at top of CuO. The highest photocurrent density of -2.14mA/cm^2 was obtained and this photocathode also showed better stability in comparison to the CuO photoelectrode. The p-n heterojunction was formed between CuO and MoS_2 and was responsible for better charge separation efficiency. In addition to this, MoS_2 also acted as an electron transfer co-catalyst and NiO behaved as hole-transfer co catalyst, together these provided the better transfer of the charge carriers, thereby led to the reduction in the recombination of photogenerated charge carriers. This design also inhibited the photocorrosion of the CuO.

Wang et al (2020) had improved the PEC performance of TiO_2 by forming heterojunction with different morphologies of ß-In_2S_3. The photoelectrode was synthesized by simple hydrothermal method. The influence of the different morphologies of ß-In_2S_3 on the photoelectrochemical properties was inquired. The different morphologies were obtained at different hydrothermal preparation time such as preparation time of 6, 12, and 14 h led to tetragonal particles, wedged particles, and spherical particles, respectively, and also futher increase in preparation time has provided accumulated particles. From the experimental analysis, it was shown that the wedged particles provided the highest PEC performance. The photocurrent density was 0.82mA/cm^2 at 1 V_{SCE} under visible light illumination. The type II heterojunction provided better charge separation and extended light absorption in the visible region.

Kodan et al (2020) had synthesized a novel hydrogenated ZnO NRs/Fe_2O_3 NPs photoelectrode by nucleation controlled chemical bath deposition, hydrogen annealing and sol-gel spin coating technique. The photocurrent density of 6.8mA/cm^2 was obtained. In this heterostructure, Fe_2O_3 NPs played a critical role by behaving as a visible light trapper, which improved the light absorption by the photoelectrode. Moreover, these nanoparticles also increased the surface area of the photoeectrode. The hydrogenation of the ZnO NRs also improved the visible light absorption. At last, experimental analysis showed the formation type II heterojunction, which was responsible for the efficient charge separation and reduced recombination of the charge carriers.

Coelho et al (2020) had provided a novel, inexpensive and easily scalable method for the formation of WO_3/$BiVO_4$ heterojunction photoelectrode. In this novel method, metallic Bi was electrodeposited over WO_3 planar film prepared by spray coating method, then, NH_4VO_3 was added to form $BiVO_4$ after thermal treatment. In comparison to the other methods for heterojunction formation like drop casting, this method provided positive effect on the photocurrent density. The photocurrent density of 2.1 ± 0.3mA/cm^2 at 1.23 V_{RHE} was obtained. The heterojunction formation by electrodeposition of metallic Bi led to the improved staggered band alignment leading to the better charge separation.

Zhu et al (2020) had fabricated β-$Ni(OH)_2$@CdS shell-core nanorod array photoanode. The photoanode was prepared by hydrothermal, photodeposition and in-situ oxidation methods. The photocurrent density of 1.2mA/cm^2 under visible light irradiation was obtained (6 times than pristine CdS nanorods). The rate of hydrogen evolution was also remarkable without bias to 762.5 μmol/h. The formation of type II p-n heterojunction between β-$Ni(OH)_2$ NPs and CdS NRs led to the improved interfacial charge separation and enhanced visible light absorption. The photoluminescence measurements showed that the recombination rate of charge carriers was reduced.

Hao et al (2020) had fabricated two dimensional WO_3/$CuWO_4$ uniform core-shell heterstructure via electrodeposition-anealing method and then incorporation of Co-Pi co-catalyst was done over it. This ternary composite provided photocurrent density of 1.4mA/cm^2 at 1.23 V_{RHE}. The absorption edge extended because of the presence of $CuWO_4$, which acted as light sensitizer. The chronoamperometry studies showed that charge transport and separation efficiency improved in the ternary photoelectrode. The $CuWO_4$ shell over WO_3 prevented the corrosion of WO_3, thereby, increased the stability of the

photoelectrode for long time. The Co-Pi co-catalyst acted as the hole extractor, hence provide better separation of the photogenerated charge carriers.

Tian et al (2020) fabricated 0D/2D ZnSe/$MoSe_2$ by using simple hydrothermal method. ZnSe nanoparticles were attached on the two dimensional nanoplates to form three dimensional flower-like heterostructure. The corresponding highest photocurrent density 5.02 mA/cm^2 was obtained. The testing for specific surface area using BET was also done, which showed that this heterostructure provided large specific surface area helping in facile transfer of charge carriers. The UV-visible spectra proved that the light absorption edge was extended to full UV and visible region of the solar spectrum i.e. 200-800nm. Internal resistance measurements and fluorescence spectroscopy showed improvement in the charge transport and separation efficiency. The reason given for such enhancement in the PEC performance was the formation of the heterojunction.

Shi et al (2020) had reported a heterojunction WO_3/$ZnIn_2S_4$ formation by hydrothermal method and then surface modification of this heterostructure was done using silane molecule through chemical water bath method. The optimization of the photoelecrode was done by controlling grating amount of the silane. The optimized photoelectrode showed highest photocurrent density of 1.51mA/cm^2 at 1.23 V_{RHE} and negatively shifted onset potential. The type II staggered band alignment was there between WO_3 and $ZnIn_2S_4$, which provided efficient charge separation efficiency. Silane molecule acted as water oxidation catalyst on the surface and extract holes even from the WO_3 bulk, thereby, increasing reactive site for the reaction to take place and provided improvement in charge separation efficiency.

John et al (2020) had compared the performance of CuO/Cu_2O nanowire/nanoflake branched heterostructure with that of core/shell hetrostructure. The preparation of the different morphologies was done by using simple electrochemical anodization of Cu foil, hydrothermal preparation followed by annealing at different temperatures. In comparision to core /shell heterostructure, branched nanowire/nanoflake structure provide better performances. The highest photocurrent density of -1.9mA/cm^2 at -0.3 V *vs.* Ag/AgCl was obtained by annealing nanowire/nanoflake branched heterostructure at 250˚C. Formation of type II staggered heterojunction along with the conformal large surface area due to this branched heterostructure was the major reasons for such enhancement in the

performance. These factors allowed the better charge separation efficiency and extended light absorption.

Bashiri et al (2020) had prepared $SrTiO_3@TiO_2@Fe_2O_3$ nanorods through hydrothermal method. In this, the hierarchical structure was optimized by concentration of Sr and Fe. The optimized structure showed the highest performance with hydrogen production rate of 716μmol/h. The reasons for the improved performance were the increased carrier density, low charge transfer resistance, and long electron lifetime.

Sharma et al (2020) prepared 2D@0D $ZnO@MoS_x$ photoanode by using combination of electrodeposition technique and calcination. MoS_x acted as co-catalyst and also formed the type II heterojunction with ZnO. The maximum photocurrent density obtained by this combination of 2D thin sheet of ZnO and 0D nanoparticles of MoS_x was 2.95mA/cm^2 at 1.6V vs. RHE. The decoration of MoS_x increased the concentration of photogenerated charge carries, and provided good stability as comparison to pristine ZnO. The formation of the heterojunction also helped in the reduction in the recombination rate of the photogenerated charge carriers. And the observations were also supported by the photoluminescence spectroscopic analysis.

Li et al (2020) had synthesized Mo, W doped $BiVO_4$/partially covered-Fe_2O_3 spindles heterostructued photoanode for PEC water splitting. They had prepared this by using drop casting, and dry and calcination method and the precursor of Fe_2O_3 i.e. MIL-53 (Fe) was prepared by microwave synthesis. In this heterstructure, type I straddling band alignment was formed. Due to such kind of designing, an attempt was made to eliminate the limitation of type I heterostructure of these semiconductors, as now the holes that transferred from the VB of the $BiVO_4$ could be used to oxidize the water from the exposed part of the Fe_2O_4 spindles, thereby, reduced the chances of recombination of the photogenerated charge carriers. The effective charge separation was done and the corresponding photocurrent density was found out to be 5.4mA/cm^2 at 1.23 V_{RHE}.

Kaur et al (2020) had successfully mixed up two different strategies, heterostructure architecturing and introduction of impurity, to develop an efficient CuO/Ru-ZnO photoelectrode for PEC water splitting. The films were synthesized by using convenient spray pyrolysis and spin coating techniques. In the report, n/n heterojunction was reported between CuO and ZnO. The films were optimized by

controlling loading concentration of Ru and at 1% Ru, the highest photocurrent density of 2.04mA/cm^2 at 0.8 V_{SCE} was obtained. Clearly, the effect of the two approaches on the PEC performance was estimated by experimental analysis. The formation of heterojunction derived the photogenerated charge carriers towards respective redox reaction, hence, leading to the effective separation of charge carriers. The introduction of Ru played a very important role, as it improved the oxygen evolution reaction kinetics by acting a OER co-catalyst (due to RuO_2 formation), also it enhanced the transfer of the photoexcited charge carriers.

Gao et al (2020) had reported $Ag_3PO_4/BiVO_4$ n-n heterojunction. The SILAR and electrodeposition methods were used to fabricate this heterojunctioned photoelectrode. The deposition amount of Ag-Pi played critical role, as the highest photocurrent density 2.32mA/cm^2 at 1.23 V_{RHE} was obtained for $Ag_3PO_4/BiVO_4$, in which 40 cycles were done for deposition of Ag-Pi nanoparticles. Increasing the cycles of deposition led to the increment in the interfacial resistance of the photoelectrode. The onset potential was also shifted towards the more negative side. The heterojunction provided the better charge separation and injection efficiency, and also improved the water oxidation kinetics.

Choi et al (2020) successfully fabricated Pt/TiO_2/InAs NWs/p-Si heterojunction photocathode. The photocathode was fabricated using catalyst-free metal organic chemical vapor deposition, plasma-assisted ALD, and photoassisted electrodeposition method. At pH=7, the highest bias-free photocurrent density of 8.6mA/cm^2, anodic shift passi in onset potential and overall stability of photocathode were obtained. The ABPE was 1.97%. The nanowire design of InAs provided a efficient way to increase the semiconductor/electrolyte interfacial reaction by providing better transfer of the photogenerated electrons. Also, TiO_2 was used as the passivation layer for InAs, at the same time Pt prevented the TiO_2 from its degradation.

Tang et al (2020) had synthesized a ternary hereterostructure Cu_2O NPs/BWO/rGO. In this heterostructure, first, the synthesis of Bi_2WO_4 hydrangea like structure and decoration of rGO over it was done using simple solvothermal method and then Cu_2O nanoparticles were deposited by chemical reduction method. This outstanding hydrangea like structure of BWO provided large specific surface area. The PEC performance of the as-synthesized heterostructure was found out to be better than bare BWO, Cu_2O NPs/BWO. In this, rGO was acting as the electron mediator for Z scheme mechanism and

electron transporter thereby increasing the photogenerated charge separation efficiency. Also, the concentration of the photogenerated charge carriers was increased due to enhanced visible light absorption.

Yuo et al (2019) modified TiO_2/Bi_2WO_6/Au nanorod arrays by simple combination of solvothermal and hydrothermal method. The synthesized hierarchical structure achieved enhanced photocurrent density of 29μA/cm^2 at 1V vs Ag/AgCl under visible illumination. Also, the photostability of photoanode was 2h. This enhancement in PEC performance was attributed to the synergistic effect of the heterojunction having type II band alignment which helped in injecting electron to CB of TiO_2 from CB of Bi_2WO_6 and SPR effect of AuNPs inducing visible light absorption.

Park et al (2019) prepared AuNPs decorated ZnO-TiO_2 core-shell NWs via CVD and photodeposition methods on Si-wafer. The PEC study showed the enhanced photocurrent density of 1.63mA/cm^2 at 0.8 V vs. RHE, which was higher than pristine ZnO NWs and ZnO-TiO_2 core-shell NWs. The enhanced PEC performance was ascribed due to SPR induced visible light absorption, increased charge carrier separation due to Schottky barrier and improved charge separation and transportation due to core-shell NWs heterostructure.

Zhao et al (2019) successfully fabricated AuNPs-decorated Co_3O_4 NSs/TiO_2 NRs arrays photoanode via simple hydrothermal process and annealing treatment. The TiO_2 NRs acted as electron acceptor while Co_3O_4 nanosheets and AuNPs behaved as the visible light harvester. A heterojunction of type II band alignment was formed in this architecture. The photocurrent density of this photoanode was 0.37mA/cm^2 at 1.16 V vs RHE, which was 37 times higher than pristine TiO_2 NRs and 1.2 times higher than CO_3O_4/TiO_2 NRs. The improved PEC performance aroused due to the SPR effect of AuNPs and visible light driven ability of Co_3O_4 nanosheets.

Fu et al (2019) synthesized ZnO@Au@Cu_2O photoanode via electrochemical deposition for ZnO nanotubes and Cu_2O growth and hydrothermal reduction method for AuNPs decoration. The prepared photoanode showed an enhancement in the visible light absorption due to the LSPR effect of AuNPs and the inbuilt visible light trapping capacity of Cu_2O nanocrystals. The photocurrent density of ZnO@Au was 3.79μA/cm^2 at 0 V (higher than pristine ZnO). The PEC performance was further

improved to 8.65μA/cm^2 (2 times that of ZnO@Au nanotubes) at 0 V by Cu_2O under visible light irradiation.

Srivastav et al (2019) had shown combined effect of AuNPs and irradiation in PEC performance of $BiVO_4$.The samples were prepared by spray pyrolysis technique and irradiated with 600eV N^{2+} ion beam. AuNPs improved the photocurrent density due to the SPR effect by enhancing the light absorption and suppressing recombination of charge carriers. After the irradiation of $BiVO_4$/Au a nanourchins structure was formed which increased the photon harvesting ability. The photocurrent density of $BiVO_4$/Au irradiated with ion beam was found to be 2.54mA/cm^2, which was higher than pristine $BiVO_4$ and $BiVO_4$/Au. But the positive impact of irradiation was limited to optimum (low) fluence only.

Zhou et al (2019) had successfully embedded AgNPs with $CuWO_4$/BiOI heterojunction by using hydrothermal, CBD and SILAR method. The resulted photoanode exhibited a remarkably enhanced PEC performance with photocurrent density of 2.10mA/cm^2 at 1.23 V vs. RHE, which was higher than pristine (0.47mA/cm^2) and $CuWO_4$/BiOI heterojuntion. The improved performance was explained considering two aspects, one was the p-n heterojunction formation leading to carrier separation and transport via internal electric field, second was the SPR-induced hot electron injection (HEI) and plasmon resonance energy transfer (PRET) facilitating charge accumulation on both $CuWO_4$ and BiOI and suppressing charge recombination.

Yao et al (2019) fabricated MoO_3/Ag/TiO_2 nanotube photoanode via the sequence of processes including anodization of TiO_2 nanotubes, thermo-decomposition of $AgNO_3$ on TNTs, and sublimation of MoO_3. The as-synthesized photoanode (containing 0.4g of MoO_3) showed photocurrent density of 21.29μA/cm^2 at a bias of 0 V_{SHE} under visible light illumination, which was higher than bare TNTs, further increased amount of MoO_3 decreased the photocurrent density. It was suggested that the enhanced PEC performance was due to the formation of heterojunction separating electron hole pairs, plasmonic effect of Ag NPs enhancing visible light trapping, and also the injection of electron from AgNPs to both TiO_2 and MoO_3 by SPR effect and injection of electrons from VB of TiO_2 to CB of MoO_3.

Sharma et al (2019) synthesized Ag/Bi_2S_3 nanoflower photoanode via simple hydrothermal and chemical route. This nanostructured photoanode was showing a photocurrent density of 12.34mA/cm^2 at 2V vs Ag/AgCl under light exposure (100 mW/cm^2), which was higher than pristine Bi_2S_3, Bi_2S_3 nanorods, Bi_2S_3 nanoflower and Ag/Bi_2S_3 nanorods. Firstly, as compared to nanorods, nanoflowers provide more reaction sites. Secondly, the enhancement was due to the increased absorption, accelerated charge transfer by hot electrons injection, higher charge separation.

Reddy et al (2019) successfully modified yttrium-doped α-Fe_2O_3 with plasmonic Ag nanowires as a bottom layer via hydrothermal and polyol technique. After the decoration of Ag nanowire, the photoanode showed a photocurrent density 0.81mA/cm^2, which was higher than bare Fe_2O_3, and doped-Fe_2O_3. This enhancement was attributed to the reduction in band gap due to doping, decreased charge transfer resistance, increased charge separation, and low recombination rate.

Lan et al (2019) designed a $ZnFe_2O_4$/Ag/AgS photoanode by hydrothermal, chemical water bath and SILAR method. This photoanode showed a photocurrent density of 0.91mA/cm^2 at 1.23 V_{RHE} (9.10 times higher than pristine $ZnFe_2O_4$). Further, the photocurrent density was increased to 1.81mA/cm^2 by using co-catalyst Co-Pi. Overall increase in the PEC performance was attributed to the SPR-mediated hot electron injection, effective charge separation and inhibition of recombination of charge carriers. Co-Pi also prevented from photoanode from the photo-corrosion.

Sang et al (2019) prepared Cu NPs-decorated TiO_2 nanotube arrays via anodization followed by pulse electrochemical deposition method, the size of NPs was optimized by varying the deposition cycles. On 3600 cycles, Cu NPs with 30nm size were decorated on TNTAs. At this composition the Cu NPs decorated TNTAs showed a strongest SPR characteristic absorption peak. The photocurrent density obtained by this photoanode was 0.41mA/cm^2 at 0 V vs. Ag/AgCl (33% higher than pristine TNTAs). This enhancement was ascribed to the increased absorption of visible light, hot electron injection, reduced recombination rate of charge carriers, decreased charge transfer resistance. The hydrogen evolution ate were also calculated and this photoanode maintained highest rate of 15.59 µL/h-cm^2 during irradiation of 2 h. In addition, plasmonic effect of Cu NPs was compared with that of Ag NPs and no considerable different was seen.

Pawar et al (2019) had modified $LaFeO_3$ photocathode with plasmonic Ni NPs. Spray pyrolsis method was adopted for preparation of $LaFeO_3$ and decoration of Ni NPs was done by using spin coating method. The FDTD simulation were done to optimize the size of Ni NPs for better SPR effect, and the study showed that NiNPs with size between 70-100 nm had good SPR effect. Now, when the loading amount of Ni NPs was 2.84 mmol, the highest photocurrent density of 0.066mA/cm^2 at 0.6 V vs. RHE was obtained, which was almost 2 times than un-decorated $LaFeO_3$ (0.036 mA/cm^2). Chronoamperometric measurements showed that at 0 V, both photocathode (decorated and un-decorated) exhibited good stability for 20h under continuous illumination showing that stability of photocathode was not affected by Ni NPs decoration . This improved performance after decoration was ascribed to the SPR effect of Ni NPs leading to effective light absorption.

He et al (2019) prepared Pd-decorated TiO_2 nanowires photoanode via hydrothermal and electrospray technique. The size and distribution of Pd NPs on surface of TiO_2 were controlled by varying the temperature of the substrate material and volume of the precursor. The uniform distribution and size were optimized at 450º C and 200µL (precursor solution), at these value homogeneous dispersion of 5nm Pd NPs was obtained. The resulted photoanode (Pd/TiO_2) showed an enhanced photocurrent density of 1.4mA/cm^2 at 1.23 V vs. RHE, which was 5 times than the pristine TiO_2 (0.25mA/cm^2). The absorption spectra showed that this enhancement is not due to the absorption of the light because there was no significant change in absorption after Pd decoration. The IPCE measurements showed value of 22% at 380nm after decoration suggesting the enhanced charge transfer at electrode/electrolyte interface, which confirmed by EIS, Mott Schottky investigations. Higher charge density was there in case of Pd/TiO_2.

Bhat et al (2019) successfully prepared 1D (nanorod)/0D (nanocrystal)/2D nanosheet TiO_2/CdS/MoS_2 heterostructure to provide efficient photoelectrochemical performance. The formation of TiO_2 was one by hydrothermal method, followed by the chemical bath deposition technique to deposit CdS and MoS_2 over it. The as-prepared heterostructure provided the photocurrent density of 3.45mA/cm^2 at 0.9 V_{RHE}. The corresponding onset potential was negatively shifted. Due to the formation of type II band alignment the IPCE value was enhanced. The charge separation efficiency was improved and MoS_2

nanosheets acted as the hole-withdrawing layer, thereby, improvement in the charge transfer was there.

Long et al (2019) had successfully prepared $FeVO_4$/ZnO NRs heterojunction photoanode by using hydothermal, calcination, and spin coating technique. The photocurrent density achieved was about 2.05mA/cm^2 at 1.23 V_{RHE} (2.4 times than pristine ZnO). The formation of type II heterojunction created built-in electric field, which improved charge separation efficiency and slow down the recombination kinetics at the surface or bulk. The charge transfer kinetics was also enhanced. Additionally, the passivation by FVO also led to the increment in the photogenerated voltages and reduced the potential barrier for OER.

Yoo et al (2019) had fabricated TiO_2/CdS core shell hetrostructure by hydrothermal method with introduction of NiO_x over it surface by using magnetron sputtering. The optimized time for NiO_x deposition was evaluated to be 15 min and the remarkable photocurrent density of 30mA/cm^2 at 1 V vs. Ag/AgCl, along with this anodic shift in onset potential was also observed. The p-n heterojunction was formed between TiO_2/CdS and NiO_x. This heterojunction led to the efficient charge separation as the built-in electric field drifted the photoexcited electrons and holes oppositely.

Yoon et al (2019) had successfully incorporated MOF in PEC water splitting by synthesizing MIL(125)-NH_2/TiO_2 NRs as a photoelectrode using simple hydrothermal method. The photocurrent density of 1.63mA/cm^2 at 1.23 V_{RHE} was observed in 1M NaOH electrolytic solution. The IPCE value was also improved to 84.4% at 340 nm (λ_{max}). The type II staggered hetrojunction was formed between TiO_2 and MIL(125)-NH_2, which significantly improve the light absorption and charge separation and transportation. This MOF/semiconductor hterojunction provided the enhanced PEC performance along with good stability without the utilization of the any co-catalyst.

Yu et al (2019) had synthesized Co_3O_4/P-C_3N_4/TiO_2 core/shell heterostructured ternary photoanode. TiO_2 NRs were prepared by simple hydrothermal method, then coating of phosphorous doped g-C_3N_4 was done over it, and finally 0D Co_3O_4 nanodots were decorated by using chemical bath deposition technique. In this heterostructure, type II band alignment was observed. The uniform decoration of Co_3O_4 nanodots provided enhancement in visible light response and short diffusion length for charge transfer, and these nanodots also acted as Oxygen evolution co-catalyst improving its kinetics. The

built-in electric field led to the efficient charge separation and reduction of recombination rate of charge carriers. The obtained photocurrent density was 1.58mA/cm^2 at 1.23 V vs. RHE.

Wang et al (2018) synthesized Au-NSs/TiO_2 NRs heterostructured photoanode. TiO_2 NRs and and Au nanostars were prepared by hydrothermal and Surfactant-free wet chemistry method respectively. This heterostructure of TiO_2 nanorods using Au-NSs provided improved PEC performance under both visible light illumination and simulated sunlight. Under simulated light, the photocurrent density of 0.95mA/cm^2 at 1.0 V vs NHE was achieved which was greater than bare TiO_2 NRs. The IPCE value in UV region was improved due to photon scattering effect of these Au- NSs and in visible NIR region because of long wavelength plasmon resonance and injection of hot electron to CB of TiO_2. So this study showed that the Au nanostars decoration provided a much better IPCE values than Au nanoparticles and Au nanorods.

Waleed et al (2018) prepared titania photoanodes with different morphologies (TNP, TNS and TNT) by simple hydrothermal method and decorated them with Au NPs (TNP@Au, TNS@Au and TNT@Au) by photoreduction method. After Au NPs decoration the PEC performance of all titania was increased. Titania nanotubes decorated with Au NPs (TNT@Au) showed highest photocurrent density of 5.19mA/cm^2 at 1V vs NHE among all of them. Also, the onset potential was shifted to more negative values after Au NPs decoration. This was attributed to the decrease in charge transfer resistance and longer lifetime of charge carriers in case of TNT@Au. This combined effect of tubular structure of titania having larger surface area, light absorption and scattering, and plasmonic effect of Au NPs had provided highest photocurrent density to TNT@Au.

Chen et al (2018) designed an Au-surface/$BiVO_4$-WO_3 heterojuntion/Au-bottom nanopatterned (antenna/spacer/reflector) photoanode via self-assembly method, sol-gel spin coating methods. The $BiVO_4$ heterojunction was sandwiched between large underlying Au nanospheres (back reflector for light) and small surface Au nanospheres (antennas for absorption of incident and reflected light). This arrangement promoted the light harvesting and absorbing ability of $BiVO_4$ spacer, and promoted charge separation and transport due to the coupled interaction of EM field between reflector and antenna. Additionally, WO_3 acted as the selective transporter of electrons and block hole-transport to Au bottom. This resulted structure had a photocurrent density of 1.31mA/cm^2 which further improved

to 1.97mA/cm^2 at 1.23 V_{RHE} by using FeOOH catalyst (which improved charge transfer at semiconductor/electrolyte interface). This enhanced efficiency was higher than bare $BiVO_4$, $BiVO_4$-WO_3, Au-surface/$BiVO_4$-WO_3, $BiVO_4$-WO_3/Au-bottom.

Kumar et al (2018) prepared Ag-decorated $NaNbO_3$ NRs photoanode by simple hydrothermal and chemical solution method. This photoanode showed enhanced photocurrent density of 3.54mA/cm^2 at 0.9 V vs Ag/AgCl almost 4 fold increased than bare $NaNbO_3$ NRs (0.74mA/cm^2). Also, this photocurrent was higher than the previously reported photocurrent density of other metal/semiconductor combination. The enhanced PEC performance was ascribed to the surface plasmon mediated electron transfer from AgNPs to the CB of $NaNbO_3$ NRs, enhanced absorption in visible light region, and reduction in the recombination rate of the photoexcited charge carriers.

Sang et al (2018) fabricated Ag/TiO_2 naotubes photoanode by anodization and pulse-electrodeposition technique. The size and amount of the AgNPs were controlled by deposition-charge density. Three samples were prepared at 300, 600 and 1200mC/cm^2 denoted as Ag/TNT-300, Ag/TNT-600 and Ag/TNT-1200, respepctively. The size and amount was increasing with increase in deposition-charge density, and at 600mC/cm^2 highly distributed AgNPs with diameter 10-50 were obtained. The UV-Vis diffused reflectance spectra suggested that Ag/TNT-300 was having a great SPR peak at 400-465 nm. But Ag/TNT-600 was showing highest photocurrent density (0.45mA/cm^2 0 V vs Ag/AgCl) and hydrogen production rate under simulated solar illumination (AM 1.5, 100 mW/cm2), and higher IPCE values at 300-400 nm range indicating that better reduction in recombination rate. Additionally, under visible light illumination Ag/TNT showed lower photocurrent density (0.0066mA/cm^2) suggesting that SPR effect-mediated hot electron injection have only limited role in enhancement of PEC performance. The IMPS measurements suggested SPR-induced localized electronic field facilitated electron transport enhancing interfacial charge transfer.

Wang et al (2018) decorated Ni nanopaticles on black TiO_2 nanowires photoanode. The black TiO_2 NWs were synthesized by hydrothermal followed by hydrogenation, and Ni NPs were deposited using ALD method. The size and loading amount of Ni NPs were optimized by preparing samples through different number of cycles. At 50 cycles, optimized size and uniform distribution of NPs was obtained, and further increasing the number of cycles to 100 the Ni NP deposition became non-uniform. The

highest photocurrent density of 0.165mA/cm^2 at 0.23 V vs. Ag/AgCl under visible light illumination was obtained for 50 cycle- Ni/black TiO_2 NWs. The reasons given for this enhancement were: increment in the carrier concentration and visible light absorption by SPR of Ni NPs, suppression of the recombination rate of charge carriers due to formation of the schottky barrier.

Li et al (2018) synthesized a heterostructured Al@TiO_2 nanocavity arrays photoanode via anodization, e-beam evaporation and thermal dewetting methods. The highest photocurrent density was seen for Al@TiO_2 having 20nm Al layer with Al NPs (size~34nm), which was approx. 2-3 times higher than the bare TiO_2 at 1.23 V vs. RHE under UV-visible light and further increase in particle size decreased the photocurrent density. This showed the effect of size of Al NPs on the photo-activity. All investigation including SERS, IPCE, potential decay curve, EIS, FDTD simulation revealed that this enhancement resulted from the LSPR-induced electromagnetic field enhancement in UV-visible region and photo-induced hot carrier injection. The naturally formed Al_2O_3 layer acted as a protective layer preventing Al NPs corrosion and reduced the surface charge recombination.

Choi et al (2017) fabricated Au NP-decorated TNT photoanode by two-step anodization process followed by agglomeration of Au NPs. The 2nd anodized TNT showed high photocureent density of 0.62mA/cm^2 at 1.23 V vs. RHE, low onset potential and photostability than 1st anodized TNT and this was attributed to the more efficient charge separation and transportation due to reduced cracking and high crystallinity. In addition, decoration of Au NPs to the surface of 2nd anodized TNT had improved the photocurrent density to 1.02mA/cm^2 at 1.23 V vs. RHE due to LSPR effect of plasmonic AuNPs.

Subramanian et al (2017) synthesized AuNPs/GQDs-decorated TiO_2 nanorod photoanode. TiO_2 nanorods prepared by simple hydrothermal method, Au NPs deposited on TNRs via facile layer adsorption and thermal reduction method and GQDs deposited through simple impregnation method. This photoanode showed photocurrent density of 1.7mA/cm^2 at 1.2 V vs RHE. The improved PEC performance was attributed to the PRET/SPR-induced hot electron injection of AuNPs and also to the electron injection from CB of GQDs to CB of TiO_2. This improved performance was not only due to individual effect of AuNPs and GQDs but also due to the synergistic effect of both as this combination showed unique phenomenon of Exciton-Plasma interaction (EPI).

Zhou et al (2017) prepared highly ordered 3D Au-decorated $BiVO_4/SnO_2$ inverse opal structure via template-assisted, swell-to-shrink hydrothermal technique. The inverse opal structure provided large surface area, and the heterojunction between $BiVO_4$ and SnO_2 having a matched band gap energy structure was benefactor to facilitate charge separation. The light harvesting ability was increased due the overlapping the slow photon effect of inverse opal which amplified the and SPR effect of AuNPs. The Au-$BiVO_4/SnO_2$ displayed photocurrent density of 3.83mA/cm^2 at 1.23 V vs RHE (3 times higher than planar $BiVO_4$).

Ng et al (2017) investigated the impact of different arrangement of plasmonic AuNPs and WO_3 photoanode on the photoelectrochemical properties. The four configurations were prepared via electrodeposition method denoted as Pristine WO_3, WO_3/Au-bottom layer, Au-surface layer/WO_3 and Au/WO_3/Au sandwiched configuration. Although, the sandwiched configuration showed the highest photocurrent density of 1.4mA/cm^2 at 1 V_{SHE} which was highest among all configurations and earlier reported photocurrent densities at this bias, but WO_3/Au photoanode showed highest ABPE conversion efficiency at low bias of 0.5 V as sandwiched structure required higher bias to generate higher photocurrent density.

Chaudhary et al (2017) successfully synthesized Ag-decorated/TiO_2/CNT ternary photoanode via hydrothermal and soft chemical route. This ternary photoanode showed enhanced photoelectrochemical properties and increased visible light absorption. In comparison to binary composite (TiO_2/CNT) this system showed four times greater photocurrent density (0.91mA/cm^2 at1.2 V) under visible light illumination. Here, CNT layer acted as an electron reservoir and facilitated charge separation and transportation. Also, due to the SPR effect of AgNPs there was enhancement in visible light absorption, low recombination rate of electron hole pair and higher charge carrier density of the ternary composite.

Hong et al (2017) fabricated Co_3O_4 photocathode with different nanostructures (naowires and nanolayers) decorated with AgNPs via simple hydrothermal and annealing process. The result showed that both Co_3O_4 NWs and NLs exhibited almost similar photocurrent densities of -0.5mA/cm^2 and -0.45mA/cm^2 at −0.4V vs. Ag/AgCl, respectively, these photocurrent densities were improved up to -4.73mA/cm^2 and -4.26mA/cm^2 by decorating with AgNPs. AuNPs acted as electron trapper

facilitating separation and transportation of charge carriers. This enhancement was ascribed to increased photoresponse in visible light, fast charge transfer leading to suppression of recombination of electron-hole pairs. Moreover, the highest photocurrent in case of nanowire was attributed to the availability of high surface-to-volume ratio and direct charge transport pathways.

Peng et al (2017) synthesized Ag/TiO_2 NWs photoaode via combining facile hydrothermal and chemical deposition method. The synthesized photoanode showed the remarkable PEC performance under visible light irradiation. The photocurrent density of 18 $\mu A/cm^2$ was achieved at -0.2 V while TiO_2 nanowire alone was not able to harvest visible light. This enhancement was attributed to the SPR-mediated electron transfer from AgNPs to CB of TiO_2 and schottky barrier which helped in preventing back flow of electrons to AgNPs.

Wang et al (2017) successfully fabricated Bi/$BiVO_4$ photoanode through electrochemical deposition followed by heating and photo-reduction methods. The as-prepared photoanode showed greater PEC performance than bare $BiVO_4$. The different samples of Bi/$BiVO_4$ were prepared depending upon the deposition time of 30, 60 and 90 minutes. The highest photocurrent density of 0.4mA/cm^2 was obtained for Bi/$BiVO_4$-60 photoanode at bias greater than 0.7 V vs. Ag/AgCl, which was 2 times greater than that of bare $BiVO_4$. This enhancement in the PEC performance was ascribed to the greater visible light absorption, efficient separation and transfer of charge carriers by SPR-mediated local electromagnetic field, schottky junction formation, and electron capturing ability of Bi metallic to its VB from $BiVO_4$.

Xu et al (2016) synthesized TiO_2 NRs array via seed-free and seed-assisted method. Au NPs were decorated on synthesized TiO_2 by photoreduction method. Seed-free TiO_2 NRs exhibited more prominent PEC performance than seed-asssisted TiO_2 NRs due to enhanced charge transfer efficiency. Moreover, decoration of seed-free TiO_2 with Au NPs further increased photoelectric current to 1.1mA/cm^2 at 1.0 V vs Ag/AgCl due to the SPR effect of the Au NPs which led to increase absorption edge, decrease the transfer resistance, improve electron lifetime and increase photogenerated carrier density. Also the loading of AuNPs was a crucial factor. The photocurrent density of 1.1mA/cm^2 at 1.0 V vs Ag/AgCl was for wt 2.36 % amount of loaded AuNPs, further increased loading amount decreased the photocurrent density.

Luo et al (2016) successfully modified Au/reduced graphene oxide/hydrogenated TiO_2. TiO_2 nanotube was prepared by two-step anodization followed by electrophoretic deposition of of graphene oxide layers and Au NPs. The Au/RGO/H-TNTs photoanode showed photocurrent density of 224 $\mu A/cm^2$ and IPCE of 5.8 % under visible light irradiation, which was higher than TNTs, H-TNTs and RGO/H-TNTs. This was suggested that the PEC performance increased as H-TNTs not only showed visible light absorption due to narrow band gap but also serve as electron collector, RGO middle layer act as excellent electron transporter facilitating separation of carriers, Au NPs serve as photosensitizer for visible light harvesting due to LSPR effect.

Luo et al (2016) fabricated Ligand exchange assisted plasmonic Au/TiO_2 nanotubes(LE-Au/TNTs) photoanode for visible light harvesting. It was formed by depositing self-assembled monolayer of MPA inside TNTs (prepared via two-step anodization process) and then substitute the ligand on the surface of AuNPs (prepared via seeded growth method) through direct ligand exchange method. Under visible light illumination, the photocurrent density and IPCE of LE-Au/TNTs was found to be 202$\mu A/cm^2$ at 1.23 V vs. RHE and 7.4 % (at 555nm), which were higher than pristine TNTs and PI-Au/TNTs (prepared via impregnation precipitation). This enhancement was attributed to the LSPR effect of AuNPs which induced strong visible light absorption and well stabilized schottky barrier which was beneficial for charge separation and transfer.

Fan et al (2016) prepared TiO_2/Au/PTh photoanode on FTO via simple hydrothermal and electrodeposition method. TiO_2 served as supporting platform, polythiophene (PTh) a organic polymer acted as visible light harvester and plamonoic AuNPs formed bridge between PTh and TiO_2 to generate more electron hole pair, accelerate electron transport which help in charge separation between them and also improved visible light absorption. Due to all these effects, the PEC performance was increased to 0.24mA/cm^2at 0.8V (Ag/AgCl) under visible light irrradiation and chemical stability of photoanode was increased.

Zhang et al (2016) designed Au-decorated two-story CdSe@RGO+CdSe@ZnO hetero-nanostructured photoanode. ZnO NRs formed via simple hydrothermal method, CdSe coating was done via CBD method. The photocurrent density of this photoanode was reached to 10.74mA/cm^2 at 0 V SHE under white light illumination. This enhancement was ascribed to the effective plasmonic interaction

between Au and CdSe and between Au and ZnO as it increased visible light absorption due to schottky junction and hot electron injection, respectively. Additionally, efficient charge separation and transport due to formation of type II band alignment of CdSe/ZnO.

Cao et al (2016) designed nanostructured photoanode in which $ZnFeO_3$ (ZFO) nanoparticles were deposited over CdS QDs/ZnO NRs core/shell structure. This composite contained type II heterojunction between these three units, which improved the charge separation efficiency and also the quantum dot sensitization along with deposition of ZFO increased the light absorption ability of photoanode. Moreover, ZFO acted as hole-extractor and passivation support for photo-corrosive CdS quantum dots. The result of this combination was remarkable with photocurrent density of 3.88mA/cm^2 at 0V vs Ag/AgCl and STH efficiency of 4.4 %.

Guo et al (2015) designed a unique heterostructured photoanode TiO_2/Ag/Ag_2S/Ag_3CuS_2 NRs via hydrothermal, SILAR, and simple ion exchange method. The as-synthesized photoanode involved simultaneous effect of plasmonic noble metal, and sensitization with binary metal sulfide (Ag_2S) and ternary metal sulfide (Ag_3CuS_2). This photoanode showed a photocurrent density of 2.27mA/cm^2 at 0 V vs Ag/AgCl, which was 2 times higher than pristine TiO_2 NRs. The resulted performance was due to the enhanced light absorption because of multiple sensitization, increased charge separation, and increased charge transfer because of SPR effect of Ag nanoparticles.

Nishanthi et al (2015) prepared Ag decoated-TiO_2 nanotube photoanode by electrochemical anodization and photochemical reduction approach. The visible light absorption was enhanced in the absorption range 430-600 nm with characteristic absorbance at about 500 nm owning to the SPR effect of Ag nanoparticles. PL spectra of Ag/TiO_2 nanotube showed lowest intensity than bare TiO_2 nanotube, indicating greater charge separation, long lifetime of charge carrier and low recombination. Considering all these enhancement, the observed saturated photocurrent density of 5.13 mA/cm^2 in presence of hole scavenger was obtained for the sample Ag/TiO_2-3-05 with and optimum loading of Ag NPs (3h deposition time and 5 min UV irradaiation time).

Xu et al (2015) had fabricated a photoanode Au decorated/WO_3 nanorod arrays via hydrothermal and photoreduction method. The resulted photoanode showed an enhanced photocurrent density of 1.17mA/cm^2 at 1.0 V vs Ag/AgCl, which was higher than that of bare WO_3 nanorod. Also the

photoanode showed a cathodic shift in the onset potential of 0.2 V, photoconversion efficiency was almost 10 times higher than that of bare WO_3 nanorod, and the stability of the photonaode was also increased after Au decoration. The reasons for these improvements could be observe from the absorption spectra, EIS and Mott Schottky measurements. These measurements suggested high light absorption, fast electron transport and high charge carrier density due to the SPR effect of Au NPs.

Zhang et al (2015) had synthesized unique arrangement of photoanode containing Au-decorated ZnO nanorod@nanoplatelet core-shell nanoarray throughfacile hydrothermal and photoreduction method. The SPR of Au NPs enhanced the visible light absorption in range 500-600 nm. The highest photocurrent density was observed to be 1.47mA/cm^2 at 0.6 V, which was higher than pristine ZnO NR (0.8 mA/cm^2) and ZnO NR@NP core-shell (1.17 mA/cm^2). The reasons given were better light absorption, good charge separation, fast charge transfer, and also the result of DFT study which showed transfer of electrons from ZnO to Au helping in low recombination rate. Visible light assisted IPCE value was also increased after Au decoration due to SPR effect. Additionally, this core-shell nanostructure provided good light harvesting capacity.

Chen et al (2013) had been prepared Ag NPs-decorated TiO_2 nanotube arrays through electrochemical anodization followed by photochemical reduction method. The silver nanoparticle's size dependent investigation was done. Different irradiation time in photochemical reduction method allowed deposition of different size of Ag NPs on TiO_2 NTAs such as irradiation time of 15, 30, 60, and > 60 min led to the deposition of Ag NPs of sizes 30, 60, 90, upto 100 nm. DRS spectra showed that the sample in which irradiation time was 15 min had shown enhanced visible light absorption than other samples due to LSPR effect of silver nanoparticles ascribed to the small size. PL spectra showed that Ag decorated samples had low PL intensity than bare TiO_2, and PL intensity decreased as the size of Ag NPs decreased in sample indicating better charge separation. The photocurrent density and photoconversion efficiency of this sample was also higher than other samples having a value of 35.52uA/cm^2 and 0.056% at 0.6 V_{SHE}. So, they concluded that size of metal nanoparticles can tune plasmonic properties of them.

Li et al (2013) had synthesized a photoanode decorated with gold nanoparticles having configuration Au/TiO_2/Au through hydrothermal method followed by constant current electrodepostion method.

This configuration provided highest performance than single configuration. The Au decorated samples provided extended light absorption in the visible region due to the SPR effect of the gold nanoparticles. The as-synthesized photoanode showed photocurrent density which was 6 times higher than the pristine sample it was due to reduction in the recombination rate of charge carriers and improved light absorption.

Naseri et al (2013) had prepared WO_3 decorated with Ag naoparticles with different loading amount by simple and convenient sol-gel method followed by dip-coating technique. Optical density spectra of the as-prepared samples showed that characteristic SPR peak was there at 470 nm, and also increasing the loading silver nanoparticles increase the absorption edge. The PEC measurements showed that the sample having 2 mol% Ag-decoration showed the highest photocurrent density (1.5 times higher than bare WO_3), further increase in the concentration of silver nanoparticles on WO_3 surface decreased the photocurrent density. This sample also showed the highest hydrogen evolution rate of 3umol/h. The reasons given were the SPR effect-mediated visible light absorption, decreased charge transfer resistance.

Solarska et al (2012) had prepared a photoanode on FTO substrate, in which Ag NPs were embedded between FTO and WO_3, through sputtering and sol gel technique. The resulted photoanode exhibited a better PEC response (almost 60% enhancement) with optimum thickness of 4nm of Ag layer containing Ag NPs of sizes ranging from 10-50 nm. SERS (Surface-enhanced Raman Spectroscopy) experiment was done to investigate the near-electromagnetic field generated within the range of surface plasmon resonance corresponding wavelength, and the result showed that the better performance was due to the generation of enhanced electromagnetic field. Further, to investigate surface plasmon generation ability of Ag NPs, SNOM (scanning near-field optical microscope) measurements were taken into consideration, and they suggested coupling interaction between incident light and surface plasmon.

REFERENCES

- Afroz K, Moniruddin M, Bakranov N, Kudaibergenov S, Nuraje N (2018). A heterojunction strategy to improve the visiblelight sensitive water splitting performance of photocatalytic material. Journal of Material Chemistry A, 6(44), 21696-21718

- Alvi NH, Rodriguez PEDS, Hassan W, Zhou G, Willander, Notzel R (2019). Unassisted water splitting with 9.3% efficiency by a single quantum nanostructure photoelectrode. International Journal of Hydrogen Energy, 44, 19650-19657.
- Atabaev TS (2018). Plasmon-enhanced solar water splitting with metal oxide nanostructure: A brief overview of recent trends. Frontiers of Material Sciences, 12, 207-213.
- Bai S, Tian K, Meng JC, Zhao Y, Sun J, Zhang K, Feng Y, Luo R, Li D, Chen A (2020). Reduced graphene oxide decorated SnO_2 /$BiVO_4$ photoanode for photoelectrochemical water splitting. Journal of Alloys and Compounds, 855, 156780.
- Bashiri R, Irfan MS, Mohamed NM, Sufian S, Ling LY, Suhaimi NA, Samsudin MFR (2020). Hierarchically $SrTiO_3$@TiO_2@Fe_2O_3 nanorod heterostructures for enhanced photoelectrochemical water splitting. https://doi.org/10.1016/j.ijhydene.2020.02.106.
- Begal IV, Chodankar NR, Hassan MA, Waseem A, Johar MA, Kim DH, Ryu SW (2019). Cu_2O as an emerging photocathode for solar water splitting-A status review. International Journal of Hydrogen energy, 44(39), 21351-21378.
- Bhat SSM, Pawar SA, Potphode D, Moon CK, Suh JM, Kim C, Choi S, Patil DS, Kim J, Shin JC, Jang HW (2019). Substantially enhanced photoelectrochemical performance of TiO_2 nanorods/CdS nanocrystals heterojunction photoanode decorated with MoS_2 nanosheets. Applied Catalysis B: Environmental, 259, 118102.
- Cai J, Shen J, Zhang X, Ng YH, Huang J, Guo W, Lin C, Lai Y (2019). Light-Driven sustainable hydrogen production utilizing TiO_2 nanostructures: A Review. Small Methods, 3(1), 1800184-1800207.
- Cao S, Yan X, Kang Z, Liang Q, Liao X, Zhang Y (2016). Band alignment engineering for improved performance and stability of $ZnFe_2O_4$ modified CdS/ZnO nanostructured photoanode for PEC water splitting. Nano Energy, 24, 25-31.
- Chaudhary D, Singh S, Vankar VD, Khare N (2017). A ternary Ag/TiO_2/CNT photoanode for efficient photoelectrochemical water splitting under visible light irradiation. International Journal of Hydrogen Energy, 42(12), 7826-7835.

- Chen B, Zhang Z, Baek M, Kim S, Kim W, Yong K (2018). An antenna/spacer/reflector based Au/$BiVO_4$/WO_3/Au nanopatterned photoanode for plasmon-enhanced photoelectrochemical water splitting. Applied Catalysis B: Environmental, 237, 763-771.
- Chen D, Liu Z, Guo Z, Yan W, Ruan M (2020). Decorating Cu_2O photocathode with noble-metal-free Al and NiS cocatalysts for efficient photoelectrochemical water splitting by light harvesting management and charge separation design. Chemical Engineering Journal, 381, 12655.
- Chen K, Feng X, Hu R, Li Y, Xie K, Li Y, Go H (2013). Effect of Ag nanoparticle size on the photolectrochemical properties of Ag decorated TiO_2 nanotube arrays. Journal of Alloys and Compounds, 554, 72-79.
- Choi S, Hwang J, Lee TH, Kim HH, Hong SP, Kim C, Choi MJ, Park HK, Bhat SSM, Suh JM, Lee J, Choi KS, Hong SH, Shin JC, Jang HW (2019). Photoelectrochemical Hydrogen Production at Neutral pH Phosphate Buffer Solution Using TiO_2 Passivated InAs Nanowire/*p*-Si Heterostructure Photocathode. Chemical Engineering Journal, 392, 123688.
- Choi YJ, Sung HY, Choi JH, Kim DY, Huh D, Lee H (2017). Fabrication of Au nanoparticle-decorated TiO_2 nanotubes arrays for stable photoelectrochemical water splitting by two-step anodization. Ceramics International, 43(16), 14063-14067.
- Christopher P, Ingram DB, Linic S (2010). Enhancing photochemical activity of semiconductor nanoparticles with optically active Ag nanostructures: Photochemistry mediated by Ag surface plasmons. The Journal of Physical Chemistry C, 114(19), 9173–9177.
- Coelho D, Gaudêncio JPRS, Carminati SA, Ribeiro FWP, Nogueira AF, Mascaro LH (2020). Bi electrodeposition on WO_3 photoanode to improve the photoactivity of the WO_3/$BiVO_4$ heterostructure to water splitting. Chemical Engineering Journal, 399, 125836.
- Cui W, Shang J, Bai H, Hu J, Xu D, Ding J, Fan W, Shi W (2020). In-situ implantation of plasmonic Ag into metal-organic frameworks for constructing efficient Ag/NH_2-MIL-125/TiO_2 photoanode. Elsevier Chemical Engineering Journal, 388, 124206.
- Djurišić AB, He Y, Ng AMC (2020). Visible-light photocatalysts: Prospects and challenges. APL Materials, 8(3), 030903.

- Esmaeili-Zare M, Behpour M (2020). CIS/CdS/ZnO/ZnO:Al modified photocathode for enhanced photoelectrochemical behavior under visible irradiation: Effects of pH and concentration of electrolyte solution. International Journal of Hydrogen Energy, 45, 8273-8281.
- Fan W, Chen C, Bai H, Luo B, Shen H, Shi W (2016). Photosensitive polymer and semiconductors bridged by Au plasmon for photoelectrochemical water splitting. Applied Catalysis B: Environmental, 195, 9-15.
- Fu S, Chen J, Han H, Wang W, Shi H, Fu J, Jia Y (2019). ZnO@Au@Cu_2O nanotube arrays as efficient visible-light-driven photoelectrod. Journal of Alloys and Compounds, 799, 183-192.
- Fujishima A and Honda K (1972). Electrochemical photolysis of water at a semiconductor electrode. Nature, 238, 37-38.
- Gao J, Sun X, Wang Y, Li Y, Li X, Chen C, Ni J (2020). Ultrathin Al_2O_3 passivation layer-wrapped Ag@TiO_2 nanorods by atomic layer deposition for enhanced photoelectrochemical performance. Applied Surface Science, 499, 143971.
- Gao Y, Li X, H J, Fan W, Wang F, Xu D, Ding j, Bai H, Shi W (2020). Ag-Pi/$BiVO_4$ heterojunction with efficient interface carrier transport for photoelectrochemical water splitting. Journal of Colloid and Interface Science, 579, 619-627.
- Ghobadi TGU, Ghobadi A, Karadas F, Ozbay E (2020). Large scale compatible fabrication of gold capped titanium dioxide nanoantennas using a shadowing effect for photoelectrochemical water splitting. International Journal of Hydrogen Energy, 45(3), 1521-1531.
- Guo K, Liu Z, Han J, Zhang X, Li Y, Hong T, Zhou C (2015). Higher-efficiency photoelectrochemical electrodes of titanium dioxide-based nanoarrays sensitized simultaneously with plasmonic silver nanoparticles and multiple metal sulfides photosensitizers. Journal of Power Sources, 285, 185-194.
- Guo Z, Wei J, Zhang Bo, Ruan M, Liu Z (2020). Construction and photoelectrocatalytic performance of TiO_2/$BiVO_4$ heterojunction modified with cobalt phosphate. Journal of Alloys and Compounds, 821, 153225.

- Han Y, Yao CB, Cai Y, Bao SB, Jiang GQ (2020). Copper decorated ZnO nanowires material: Growth, optical and photoelectrochemical properties. Journal Of Alloys and Compounds, 835, 155339.
- Hao Z, Liu Z, Li Y, Ruan M, Guo Z (2020). Enhanced photoelectrochemical performance of 2D core-shell WO_3/$CuWO_4$ uniform heterojunction via in situ synthesis and modification of Co-Pi cocatalyst. International Journal of Hydrogen Energy, 45(33), 16550-16559.
- He J, Wang M, Wu X, Sun Y, Huang K, Chen H, Gao L, Feng S (2019). Influence of controlled Pd nanoparticles decorated TiO_2 nanowire arrays for efficient photoelectrochemical water splitting. Journal of Alloys and Compounds, 785, 391-397.
- Hong T, Liu Z, Zheng X, Zhang J, Yana L (2017). Efficient photoelectrochemical water splitting over Co_3O_4 and Co_3O_4/Ag composite structure. Applied Catalysis B: Environmental, 202, 454-459.
- Huang J, Liu T, Wang R, Zhang M, Wang L, She H, Wang Q (2020). Facile loading of cobalt oxide on bismuth vanadate: Proved construction of p-n junction for efficient photoelectrochemical water oxidation. Journal of Colloid and Interface Science, 570, 89-98.
- Huynh HQ, Pham KN, Phan BT, Tran CK, Lee H, Dang VQ (2020). Enhancing visible-light-driven water splitting of ZnO nanorods by dual synergistic effects of plasmonic Au nanoparticle and Cu dopants. Journal of Photochemistry & Photobiology, A: Chemistry, 399, 112639.
- Jiang H, Chen Y, Li L, Liu H, Ren C, Liu X, Tian G (2020). Hierarchical ZnO nanorod/$ZnFe_2O_4$ nanosheet core/shell nanoarray decorated with PbS quantum dots for efficient photoelectrochemical water splitting. Journal of Alloys and Compounds, 828, 154449.
- John S, Roy SC (2020). CuO/Cu_2O nanoflake/nanowire heterostructure photocathode with enhancedsurface area for photoelectrochemical solar energy conversion. Applied Surface Science, 509, 144703.
- Kaur G, Divya, Satsangi VR, Dass S, Shrivastav R (2020). 3D-nano-hetero-structured n/n junction, CuO/Ru-ZnO thin films, for hydrogen generation with enhanced photoelectrochemical performances. International Journal of Hydrogen Energy, 41(45), 21051-21067.

- Kegel J, Povey LM, Pemble ME (2018). Zinc oxide for solar water splitting: A brief review of the material's challenges and associated opportunities. Nano energy, 54, 409-428.
- Kodan N, Ahmad M, Mehta BR (2020). Enhanced photoelectrochemical response and stability of hydrogenated ZnO nanorods decorated with Fe_2O_3 nanoparticles. Journal of Alloys and Compounds, 845, 155650.
- Kumar D, Sharma S, Khare N (2020). Piezo-phototronic and plasmonic effect coupled Ag-$NaNbO_3$ nanocomposite for enhanced photocatalytic and photoelectrochemical water splitting activity. Renewable Energy, https://doi.org/10.1016/j.renene.2020.09.132.
- Kumar D, Singh S, Khare N (2018). Plasmonic Ag nanoparticles decorated $NaNbO_3$ nanorods for efficient photoelectrochemical water splitting. International Journal of Hydrogen Energy, 43(17), 8198-8205.
- Lan Y, Liu Z, Liu G, Guo Z, Ruan M, Rong H, Li X (2019). 1D ZnFe2O4 nanorods coupled with plasmonic Ag, Ag_2S nanoparticles and Co-Pi cocatalysts for efficient photoelectrochemical water splitting. International Journal of Hydrogen Energy, 44, 19841-19854.
- Lee JB, Choi S, Kim J, Nam YS (2017). Plasmonically-assisted nanoarchitectures for solar water splitting: Obstacles and breakthroughs. Nano Today, 16, 61-81.
- Li J, Li J, Yuan H, Zhang W, Jiao Z, Zhao S (2020). Modification of BiVO4 with partially covered α-Fe_2O_3 spindles serving as hole-transport channels for significantly improved photoelectrochemical performance. Chemical Engineering Journal, 398, 125662.
- Li L, Feng K, Huang D, Wang K, Li Y, Guo Z, Ng YH, Jiang F (2020). Surface plasmon resonance effect of a Pt-nano-particles-modified TiO_2 nanoball overlayer enables a significant enhancement in efficiency to 3.5% for a Cu_2ZnSnS_4-based thin film photocathode used for solar water splitting. Chemical Engineering Journal, 396, 125264.
- Li Y, Yu H, Zhang C, Li F, Li G, Shao Z, Yi B (2013). Enhancement of photoelectrochemical response by Au modified in TiO_2 nanorods. International Journal of Hydrogen Energy, 38(29), 13023-13030.

- Li Z, Shi L, Franklin D, Koul S, Kushima A, Yang Y (2018). Drastic enhancement of photoelectrochemical water splitting performance over plasmonic Al@TiO_2 heterostructured nanocavity arrays. Nano Energy, 51, 400-407.
- Liu Z, Wu J, Zhang J (2016). Quantum dots and plasmonic Ag decorated WO_3 nanorod photoanodes with enhanced photoelectrochemical performances. International Journal of Hydrogen Energy, 41(45), 20529-20535.
- Liu Z, Zhang J, Hong T, Zheng X, Guo K, Liu Z (2016). High-efficiency nanorod-nanosheet arrays sandwich photoelectrode for photoelectrochemical water splitting. International Journal of Hydrogen Energy, 41(31), 13359-13367.
- Long X, Gao L, Li F, Hu Y, Wei S, Wang C, Wang T, Jin J, Ma J (2019). Bamboo shoots shaped $FeVO_4$ passivated ZnO nanorods photoanode for improved charge separation/transfer process towards efficient solar water splitting. Applied Catalysis B: Environmental, 257, 117813.
- Low J, Yu J, Jaroniec M, Wageh S, Al-Ghamdi AA (2017). Heterojunction Photocatalysts. Advanced Materials, 29(20), 1601694.
- Luo J, Chen J, Wang H, Liu H (2016). Ligand-exchange assisted preparation of plasmonic Au/ TiO_2 nanotube array photoanodes for visible-light-driven photoelectrochemical water splitting. Journal of Power Sources, 303, 287-293.
- Luo J, Li D, Yang Yan, Liu H, Chen J, Wang H (2016). Preparation of Au/reduced graphene oxide/hydrogenated TiO_2 nanotube arrays ternary composites for visible-light-driven photoelectrochemical water splitting. Journal of Alloys and Compounds, 661, 380-388.
- Mascaretti L, Dutta A, Kment ST, Shalaev VM, Boltasseva A, Zborˇil R, Naldoni A (2019). Plasmon-Enhanced Photoelectrochemical Water Splitting for Efficient Renewable Energy Storage. Advanced Materials, 31(31), 1805513.
- Moniz SJA, Sheylin SA, Martin DJ, Guo ZX, Tang J (2015). Visible-light driven heterojunction photocatalysts for water splitting – a critical review. Energy and Environmental Science, 8(3), 731-759.

- Mu J, Teng F, Miao H, Wang Y, Hu X (2020). In-situ oxidation fabrication of 0D/2D SnO_2/SnS_2 novel Step-scheme heterojunctions with enhanced photoelectrochemical activity for water splitting. Applied Surface Science, 501, 143974.
- Naseri N, Kim H, Choi W, Moshfegh AZ (2013). Implementation of Ag nanoparticle incorporated WO_3 thin film photoanode for hydrogen production. International Journal of Hydrogen Energy, 38, 2117-2125.
- Ng KH, Minggu LJ, Jaafara NA, Arifina K, Kassim MB (2017). Enhanced plasmonic photoelectrochemical response of Au sandwiched WO_3 photoanodes. Solar Energy Materials and Solar Cells, 172, 361-367.
- Nishanthi ST, Iyyapushpam S, Sundarakannan B, Subramanian E, Padiyan DP (2015). Plasmonic silver nanoparticles loaded titania nanotube arrays exhibiting enhanced photoelectrochemical and photocatalytic activities. Journal of Power Sources, 274, 885-893.
- Pan L, Kim JH, Mayer MT, Son MK, Ummadisingu, A, Lee JS, Hagfeldt A, Luo J, Gratzel M (2018). Boosting the performance¨ of Cu_2O photocathodes for unassisted solar water splitting devices. Nature Catalysis, 1, 412−420.
- Park J, Deshmukh PR, Sohn Y, Shin WG (2019). ZnO-TiO_2 core-shell nanowires decorated with Au nanoparticles for plasmon-enhanced photoelectrochemical water splitting. Journal of Alloy and Compounds, 787, 1310-1319.
- Patil SS, Johar MA, Hassan MA, Patil DR, Ryu SW (2018). Anchoring MWCNTs to 3D Honeycomb ZnO/GaN Heterostructures to Enhancing Photoelectrochemical Water Oxidation. Applied Catalysis B: Environmental, 237, 791-801.
- Pawar GS, Elikkottil A, Pesala B, Tahir AA, Mallick TK (2019). Plasmonic nickel nanoparticles decorated on to $LaFeO_3$ photocathode for enhanced solar hydrogen generation. International Journal of Hydrogen Energy, 44(2), 578-586.
- Peng C, Wang W, Zhang W, Liang Y, Zhuo L (2017). Surface plasmon-driven photoelectrochemical water splitting of TiO_2 nanowires decorated with Ag nanoparticles under visible light illumination. Applied Surface Sciences, 420, 286-295.

- Reddy CV, Reddy IN, Sreedhar A, Shim J (2019). Investigation of dopant and Ag plasmonic effect on α-Fe_2O_3 photoelectrode for photoelectrochemical water splitting activity. Applied Surface Science, 488, 629-638.
- Sang L, Ge H, Sun B (2018). Probing plasmonic Ag nanoparticles on TiO_2 nanotube arrays electrode for efficient solar water splitting. International Journal of Hydrogen Energy, 44(30), 15787-15794.
- Sang L, Zhang S, Gao Y (2019). Investigation of plasmonic Cu with controlled diameter over TiO_2 photoelectrode for solar-to-hydrogen conversion. Intetrnational Journal of Hydrogen Energy, 44(47), 25486-25494.
- Sharma MD, Mahala C, Basu M (2020). Sensitization of vertically grown ZnO 2D thin sheets by MoSx for efficient charge separation process towards photoelectrochemical water splitting reaction. International Journal of Hydrogen Energy, 45, 12272-12282.
- Sharma S, Kumar D, Khare N (2019). Plasmonic Ag nanoparticles decorated Bi_2S_3 nanorods and nanoflowers: Their comparative assessment for photoelectrochemical water splitting. International Journal of Hydrogen Energy, 44, 3538-3552.
- Shi X, Dong F, Dai C, Ye X, Yang P, Zheng L, Zheng H (2020). $WO_3/ZnIn_2S_4$ heterojunction photoanodes grafting silane molecule for efficient photoelectrochemical water splitting. Electrochimica Acta, 361,137017.
- Solarska R, Krolikowska A, Bienkowski K, Stefaniuk T, Augustynski J (2012). Enhancement of WO_3 performance through resonance coupling with Ag nanoparticles. Energy Procedia, 22, 137-146.
- Srivastav A, Verma A, Khan SA, Smith YR, Satsangi VR, Shrivastav R, Dass S (2019). Photoelectrochemical water splitting with 600 keV N2þ ion irradiated $BiVO_4$ and $BiVO_4$/Au photoanodes. International Journal of Hydrogen Energy, 44, 13061-13070.
- Subramanian A, Pana Z, Li h, Zhou L, Li W, Qiu Y, Xua Y, Houa Y, Muzi C, Zhang Y (2017). Synergistic promotion of photoelectrochemical water splitting efficiency of TiO_2 nanorods using metal-semiconducting nanoparticles. Applied Surface Science, 420, 631-637.

- Subramanyam P, Khan T, Sinha GN, Suryakala D, Subrahmanyam C (2020). Plasmonic Bi nanoparticle decorated $BiVO_4$/rGO as an efficient photoanode for photoelectrochemical water splitting. International Journal of Hydrogen Energy, 45 (13), 7779-7787.
- Subramanyam P, Meena B, Sinha GN, Deepa M, Subrahmanyam C (2020).Deecoration of plasmonic Cu nanoparticles on WO_3/Bi_2S_3 QDs heterojunction for enhanced photoelectrochemical water splitting. Intetrnational Journal of Hydrogen Energy, 45(13), 7706-7715.
- Subramanyam P, Meena B, Suryakala D, Deepa M, Subrahmanyam C (2020). Plasmonic nanometal decorated photoanodes for efficient photoelectrochemical water splitting. Catalysis Today, https://doi.org/10.1016/j.cattod.2020.01.041.
- Subramanyam P,Vinodkumar T, Nepak D, Deepa M, Subrahmanyam C (2018). Mo-doped $BiVO_4$@reduced graphene oxide composite as an efficient photoanode for photoelectrochemical water splitting. Catalysis Today, 325, 73-80.
- Surarez CM, Hernández S, Russo N (2015). $BiVO_4$ as photocatalyst for solar fuels production through water splitting: A short review. Applied Catalysis A: General, 504, 158-170.
- Tamirat AG, Rick J, Dubale AA, Su WN, Hwang BJ (2016). Using hematite for photoelectrochemical water splitting: a review of current progress and challenges. Nanoscale Horizons, 1, 243-267.
- Tang L, Deng Y, Zeng G, Hu W, Wang J, Zhou Y, Wang J, Tang J (2016). CdS/Cu_2S co-sensitized TiO_2 branched nanorod arrays of enhanced photoelectrochemical properties by forming nanoscale heterostructure, Journal of Alloys and Compounds, 662, 516-527.
- Tang X, Guo X, Chen Z, Liu Y, Zhang W, Wang Y, Zheng Y, Zhang M, Peng Z, Li R, Zhao Y (2020). Facile preparation of Cu_2O nanoparticles/Bi_2WO_6/rGO hybrid with enhanced photoelectrochemical performance. Applied Surface Science, 510, 145447.
- Tian P, Tang T, Zhang J, lin S, huang G, Zeng J, Kong Z, Wang H, Xi J, Ji Z (2020). High photocatalytic and photoelectrochemical performance of a novel 0D/2D heterojunction photocatalyst constructed by ZnSe nanoparticles and $MoSe_2$ nanoflowers. Ceramics International, 46(9), 13651-13659.

- Waleed MA, Rouby EI, Ahmed FA (2018). Titania morphologies modified gold nanoparticles for highly catalytic photoelectrochemical water splitting. Journal of Photochemistry and Photobiology A: Chemistry, 364, 740-749.
- Wang CC, Chou PH, Yu YH, Kei CC (2018). Deposition of Ni nanoparticles on black TiO_2 nanowire arrays for photoelectrochemical water splitting by atomic layer deposition. Electrochimica Acta, 284, 211-219.
- Wang L, Wang Y, Schmuki P, Kment S, Zboril R (2018). Nanostar morphology of plasmonic particles strongly enhances photoelectrochemical water splitting of TiO_2 nanorods with superior incident photo-to-current conversion efficiency in visible/near-infrared region. Electrochimica Acta, 260, 212-220.
- Wang Q, He J, Shi Y, Zhang S, Niu T, She H, Bi Y (2017). Designing non-noble/semiconductor Bi/$BiVO_4$ photoelectrode for the enhanced photoelectrochemical performance. Chemical Engineering Journal, 326, 411-418.
- Wang X, Li H, Zhang J, Liu X, Zhang X (2020). Wedged ß-In_2S_3 sensitized TiO_2 films for enhanced photoelectrochemical hydrogen generation. Journal of Alloys and Compounds, 831, 154798.
- Wang Y, Cao S, Huan Y, Nie T, Ji Z, Bai Z, Cheng X, Xi J, Yan X (2020). The effect of composite catalyst on Cu_2O/TiO_2 heterojunction photocathodes for efficient water splitting. Applied Surface Science, 526, 146700.
- Wang Y, Tian W, Chen C, Xu W (2019). Tungsten trioxide nanostructures for photoelectrochemical water splitting: Material engineering and charge carrier dynamic manipulation. Advanced Functional Materials, 29(23), 1809036-1809060.
- Wang Y, Wang Q, Zhan X, Wang F, Safdar M, He J (2013). Visible light driven type II heterostructures and their enhanced photocatalysis properties: a review. Nanoscale, 5(18), 8326-8339.
- Warren SC and Thimsen E (2012). Plasmonic solar water splitting. Energy & Environmental Sciences, 5, 5133-5146.

- Wen P, Sun Y, Li H, Liang z, Wu H, Zhang J, Zeng H, Geyer SM, Jiang L (2020). A highly active three-dimensional Z-scheme ZnO/Au/g-C_3N_4 photocathode for efficient photoelectrochemical water splitting. Applied Catalysis B: Environmental, 263, 118180.
- Xing H, E L, Guo Z, Zhao D, Liu Z (2020). Enhancement in the charge transport and photocorrosion stability of CuO photocathode: The synergistic effect of spatially separated dual-cocatalysts and p-n heterojunction. Chemical Engineering Journal, 394, 124907.
- Xu F, Bai D, Mei J, Wu D, Gao Z, Jiang K, Liu B (2016). Enhanced photoelectrochemical performance with in-situ Au modified TiO_2 nanorod arrays as photoanode. Journal of Alloys and Compounds, 688 Part B, 941-920.
- Xu F, Yao Y, Bai D, Xu R, Mei J, Wu D, Gao Z, Kai J (2015). A significant cathodic shift in the onset potential and enhanced photoelectrochemical water splitting using Au nanoparticles decorated WO_3 nanorod array. Journal of Colloid and Interface Science, 458, 1994-199.
- Yao L, Wang W, Liang Y, Fu J, Shi H (2019). Plasmon-enhanced visible light photoelectrochemical and photocatalytic activity of goold nanoparticles-decorated hierarchical $Ti_{O2}/B_{i2}W_{O6}$ nanorod arrays. Applied Surface Science, 469, 829-840.
- Yao Y, Sun M, Zhang Z, Lin X, Gao B, Anandan S, Liu W (2019). In situ synthesis of MoO_3/Ag/TiO_2 nanotube arrays for enhancement of visible-light photoelectrochemical performance. International Journal of Hydrogen Energy, 44, 9348-9358.
- Yaw CS, Ng WC, Ruan Q, Tang Q, Tang J, Soh AK, Chong MN (2020).Tuning of reduced graphene oxide thin film as an efficient electron conductive interlayer in a proven heterojunction photoanode for solar-driven photoelectrochemical water splitting. Journal of Alloys and Compounds, 817, 152721.
- Yaw CS, Tang J, Soh AK, Chong MN (2020). Synergistic effects of dual-electrocatalyst FeOOH/NiOOH thin films as effective surface photogenerated hole extractors on a novel hierarchical heterojunction photoanode structure for solar-driven photoelectrochemical water splitting. Chemical Engineering Journal, 380, 122501.

- Yoo I, Kalanur SS, Seo H (2019). A nanoscale p–n junction photoelectrode consisting of a NiOx layer on a TiO_2/CdS nanorod core-shell structure for highly efficient solar water splitting. Applied Catalysis B: Environmental, 250, 200-212.
- Yoon JW, Kim DH, Kim J, Jang WJ, Lee J (2019). NH_2-MIL-125(Ti)/TiO_2 nanorod heterojunction photoanodes for efficient photoelectrochemical water splitting. Applied Catalysis B: Environmental, 244, 511-518.
- Yu Z, Li Y, Qu J, Zheng R, Cairney JM, Zhang J, Zhu M, Khan A, Li W (2019). Enhanced photoelectrochemical water-splitting performance with a hierarchical heterostructure: Co3O4 nanodots anchored TiO_2@P-C_3N_4 coreshell nanorod arrays. Chemical Engineering Journal, 404, 126458.
- Zeng Y, Yang T, Li C, Xie A, Li S, Zhang M, Shen Y (2019). ZnxCd1-xSe nanoparticles decorated ordered mesoporous ZnO inverse opal with binder-free heterojunction interfaces for highly efficient photoelectrochemical water splitting. Applied Catalysis B: Environmental, 245, 469–476.
- Zhang C, Shaon M, Ning F, Xu S, Li Z, Wein M, Evans DG, DuanX (2015). Au nanoparticles sensitized ZnO nanorod@nanoplatelet core–shell arrays for enhanced photoelectrochemical water splitting. Nano Energy, 12, 231-239.
- Zhang Z, Choi C, Baek M, Deng Z, Yong K (2016). Plasmonic and passivation effects of Au decorated RGO@CdSe nanofilm uplifted by CdSe@ZnO nanorods with photoelectrochemical enhancement. Nano Energy, 21, 185-197.
- Zhao X, Wang W, Liang Y, Yao L, Fu J, Shi H, Tao C (2019). Three-dimensional plasmonic photoanode of Co_3O_4 nanosheets coated onto TiO_2 nanorod arrays for visible-light-driven water splitting. International Journal of Hydrogen Energy, 44(29), 14561-14570.
- Zheng G, Wang J, Li H, Li H, Hu P (2020). WO_3/Cu_2O heterojunction for the efficient photoelectrochemical property without external bias. Applied Catalysis B: Environmental, 265, 118561.

- Zheng X, Zhang Z, Meng S, Wang Y, Li D (2020). Regulating charge transfer over 3D Au/ZnO hybrid inverse opal toward efficiently photocatalytic degradation of bisphenol A and photoelectrochemical water splitting. Chemical Engineering Journal, 393, 124676.
- Zhou M, Guo Z, Song Q, Li X, Liu Z (2019). Improved photoelectrochemical response of $CuWO_4$/BiOI p-n heterojunction embedded with plasmonic Ag nanoparticles. Chemical Engineering Journal, 370, 218-227.
- Celebi N, Aydin MY, Soysal F, Ciftci YO, Salimi K (2021). Ligand-free fabrication of Au/TiO_2 nanostructures for plasmonic hot electron-driven photocatalysis: Photoelectrochemical water splitting and organic-dye degradation. Journal of alloys and compounds, 860, 157908.
- Zhou S, Tang R, Zhang L, Yin L (2017). Au nanoparticles coupled three-dimensional macroporous $BiVO_4$/SnO_2 inverse opal heterostructure for efficient photoelectrochemical water splitting. Electrochimica Acta, 248, 593-602.
- Zhou T, Wang J, Chen S, Bai J, Li J, Zhang Y, Li L, Xia l, Rahim M, Xu Q, Zhou B (2020). Bird-nest structured ZnO/TiO_2 as a direct Z-scheme photoanode with enhanced light harvesting and carrier kinetics for highly efficient and stable photoelectrochemical water splitting. Applied Catalysis B: Environmental, 267, 118599.
- Zhu T, Liang Y, Wang Y, Wang j, Wang W, Fu J, Yao L, Cheng Y, Han H (2020). P-type β-$Ni(OH)_2$ nanoparticles sensitize CdS nanorod array photoanode to prolong charge carrier lifetime and highly improve bias-free visible-light driven H_2 evaluation. Applied Catalysis B: Environmental, 271, 118945.